ISSN 0140 3818
SSSU 73

UNIVERSITY OF SOUTHAMPTON

DEPARTMENT OF SHIP SCIENCE

FACULTY OF ENGINEERING AND APPLIED SCIENCE

PREDICTION OF THE MANOEUVRING FORCES ON A SLENDER SHIP USING SLENDER BODY THEORY
PART I: THEORETICAL ESTIMATES OF FORCES AND MOMENTS

J.F. Wellicome, P.A. Wilson and X. Cheng

Ship Science Report No. 73
April 1994

Final Report on The Project

Prediction of The Manoeuvring Forces on a Slender Ship Using Slender Body Theory

Part I

Theoretical Estimates of Forces and Moments

by

J. F. Wellicome, P. A. Wilson

and

X. Cheng

Department of Ship Science
University of Southampton

April 1994

CONTENTS

NOTATION

a_n	Mapping function coefficients
F	Side force
F'	Non-dimensional side force
f	Side force distribution
f'	Non-dimensional side force distribution
L	Ship Length
N	Yaw moment
N'	Non-dimensional yaw moment
(n_x, n_y, n_s)	Components of the unit normal of body surface
x,y,s	Coordinates in (o,x,y,s) coordinate system
p	Pressure
q	Strength of distributed source
U	Speed of incoming flow
u,v	x and y components of flow speed
W	Complex potential
z	Complex variable z=x+iy

α	Drift angle
ρ	Fluid density
Γ	Strength of discrete vortex
Φ	Total potential of velocity
ϕ, ϕ_j	Potential of disturbance

1. INTRODUCTION

It has always be the naval architects' desire to have a convenient tool to predict the hydrodynamic characteristics of a given ship in stead of carrying out experiments to determine them which are both time consuming and expensive. Although in the foreseeable future experiment is not likely to be totally replaced by computer simulation in the field of naval architecture, the advantages are obvious in relation to the cost and time saving to use the computer's capability in the prediction of the hydrodynamic performance of a ship, especially at the design stage. However a precise mathematical model for a ship hydrodynamic problem involves the solution of 3-D Navier-Stokes equation and nonlinear free surface conditions. The present study is to develop a simplified method which can provide reasonable prediction of the manoeuvring forces on a slender ship and also can avoid tackling the N-S equation.

The present method simplifies the problem by making the following approximations:

(1) The flow is considered as inviscid and the effects of boundary layer and its separation on the forces are approximated by the introduction of a vortex shedding model.

(2) While the effect of longitudinal flow is kept in account, the flow around the ship is treated as 2 dimensional at each transverse section on the ground that the ship is slender, which implies that the interaction between sections is neglected.

(3) The free surface effect is neglected.

During the cause of the present theoretical investigation, the work has been carried out in the following aspects:

(1) A conformal mapping method to map a hull section into a unit circle, which was originally for the calculation of the side forces on the hull section and was later used for the interpolation of the hull sections.

(2) A 2-D vortex shedding model to simulate the wake and to estimate the forces on a 2-D cylindrical body caused by vortex shedding, in which discrete vortices were used to represent the body surface. This model was later extended for applying to the vortex shedding problem from a 3-D slender body.

(3) A distributed source method for the calculation of the flow velocity around a slender hull due to longitudinal flow.

Computer codes were written for each specific task. These codes were also the major components of a final code which was used to calculate the forces on a slender ship. The calculations conducted so far using this code for the drifted motion showed

some encouraging results in sway force prediction, whereas for the yaw moment, some discrepancy existed between the calculation and the measurement, which was found to be caused by the disagreement of the side force distribution in the area near the bow and stern. The reason for the disagreement was investigated and an alternative approach was suggested and tried which adopted a panel method to evaluate the contribution of the pure potential flow (without vortices) to the forces on the hull. The results showed encouraging improvement in the side force distribution.

2. A BRIEF DESCRIPTION OF THE SLENDER BODY THEORY

Let us consider a ship moving at constant speed U with a drift angle α. For convenience this can be equivalently transformed into a stationary ship in an incoming flow with an incident angle as shown in Fig.1. The side force acting on unit length of the hull can be expressed as

$$\frac{dF}{ds} = \int_c p\, n_x dl = \int_c [\, -\frac{\rho}{2} \nabla\Phi\, \nabla\Phi \,]\, n_x\, dl \qquad (1)$$

in which Φ is the total potential, c is the contour of the body section, and n_x is the x component of the unit normal of the section.

The total potential can also be written as

$$\Phi = -U\, s\, \cos\alpha + \phi_1 + \phi_2 + \phi_3$$

where ϕ_1 is the potential of disturbance to the longitudinal flow, ϕ_2 , ϕ_3 are the potentials of cross flow and external vortices respectively. Under the assumption of slender body, we have

$$|\frac{\partial\phi_j}{\partial x}|\ ,\ |\frac{\partial\phi_j}{\partial y}|\ ,\ |\frac{\partial\phi_j}{\partial s}| \ll U \qquad j = 1, 2, 3$$

Neglecting the higher order small quantities, equation (1) becomes

$$\frac{dF}{ds} = \rho\, U \cos\alpha\ \frac{d}{ds}\,[\int_c \phi_2\, n_x\, dl + \int_c \phi_3\, n_x\, dl\,]$$

$$= \rho\, U \cos\alpha\, \frac{d}{ds}[\ I_2 + I_3\ ] \qquad (2)$$

in which

$$I_2 = \int_c \phi_2\, n_x\, dl\ , \qquad I_3 = \int_c \phi_3\, n_x\, dl$$

The side force and yaw moment on the whole ship can be determined by

$$F = \int_{-\frac{L}{2}}^{\frac{L}{2}} \frac{dF(s)}{ds}\, ds = \rho\, U \cos\alpha\, [\, I_2(s) + I_3(s)\,]_{-\frac{L}{2}}^{\frac{L}{2}}$$

$$= -\rho\, U \cos\alpha\, I_3(-\frac{L}{2}) \tag{3}$$

$$N = \int_{-\frac{L}{2}}^{\frac{L}{2}} \frac{dF(s)}{ds} s\, ds = \rho U \cos\alpha\, (\, \frac{L}{2}\, I_3(-\frac{L}{2}) - \int_{-\frac{L}{2}}^{\frac{L}{2}} [\, I_2(s) + I_3(s)]\, ds\,) \tag{4}$$

Note that in deriving equations (3) and (4), it is assumed that the hull is symmetric about the y-s plane. Where the vessel is not symmetric, as would be the case with the vessel heeled in a turn, there would be a further contribution to yaw moment N from ϕ_1. Also the conditions $I_2(\pm L/2) = 0$ and $I_3(L/2) = 0$ have been used since the section areas shrink to zero at both ends of the body, and the external vortices strengths at the bow end are also zero.

It can be seen that the side force and yaw moment depend only on the cross flow potential ϕ_2 and external vortices potential ϕ_3. For a symmetric hull, the longitudinal flow affects the side force and yaw moment through external vortices and the vortex shedding model should take this effect into account.

3. CONFORMAL MAPPING METHOD

In two dimensional uniform incoming flow passing a stationary cylinder, the complex potential is well known. It is then advantagious to map a 2-D body of arbitrary shape on the physical plane z=x+iy into a unit circle on an auxiliary plane $\zeta = \xi + i\, \eta$. Theoretically a given 2-D body can be mapped into a circle by the mapping function

$$z = \sum_{n=1}^{\infty} a_n\, \zeta^{2-n} \tag{5}$$

It is obvious that the mapping function is solely decided by the coefficients a_n (n=1,2,3,...). In the present study, the approach for determining these mapping coefficients was based on a method suggested by Kerczek & Tuck (1969), but some

generalization was made to enable it to deal with asymmetric hull forms. Fig.2 shows the examples of applying the mapping method to both symmetric and asymmetric bodies including the sections of the "Mariner" hull.

For a 3-D slender body, once the mapping coefficients for each section are determined, the side force acting on per unit length can be evaluated using the following expression (J. F. Wellicome, 1981)

$$F(s,t) = -\rho\, U\frac{\partial A}{\partial s} + \rho\, \frac{\partial A}{\partial t} \tag{6}$$

in which

$$A(s) = -\,U\,\alpha\,[\,2\pi a_1(a_3 - a_1) + A_o\,]$$

where α is the drift angle and A_o is the area of hull section.

In our studies at early stage, the conformal mapping method was used and found to be effective for evaluating the sectional added mass and the side force distribution along a Mariner hull without considering the vortex shedding effect. However there are three restrictions which make this method less favourable. Firstly, some hull section profiles can not be mapped into a unit circle and therefore the mapping method will not be applicable to these sections. Secondly, without taking the vortex shedding into account, the mapping method predicts only a pure couple acting on the ship, the net side force is zero. Thirdly, mapping method is not likely to be applicable to the case of shallow water or restricted water way. In order to include the vortex shedding effect, a vortex shedding model is needed to work with the mapping method, which will greatly complicate the computation in two specific ways: (a) In order to follow through the convection of shed vortices it becomes necessary to invert the conformal mapping process to find points in the circle plane corresponding to defined points in the physical plane and (b) All the calculations of potentials and velocity components are duplicated, once for the mapping function and once for the vortices components. In principle the whole calculation in the present approach can be carried out in terms of vortex elements alone and this results in a substantial saving of programming effort.

Out of the above considerations, it was decided to adopt an alternative approach, i.e. a discrete vortex model, which takes vortex shedding into account and also undertakes the task of determining the potential of the flow field without resorting to the conformal mapping.

However, the mapping method is still useful in the interpolation of body sections, which will be discussed later in this report.

4. A 2-D VORTEX SHEDDING MODEL

This model is to simulate the vortex shedding and convection in the wake so that the viscous effect of the real flow can be taken into account.

There are three main problems to be solved in this model: (1) determining the positions of shedding points; (2) determining the strengths of nascent vortices; (3) determing the potential due to the body.

4.1 The Positions of The Shedding Points

In this model, the position where a nascent vortex separates from the body surface, i.e. the shedding point, is assumed to be at the place where the flow speed is maximum. This assumption is based on the fact that in the potential theory the maximum speed corresponds to the minimum pressure which represents the beginning of the region of adverse pressure gradient in which flow separation takes place. Although this is only an approximation--- the exact separation point is still difficult to determine theoretically at present, the predicted shedding points for a circular cylinder proved to be fairly close to experimental observations. Calculation also showed that the change in drag caused by a slight change in shedding position was negligible.

4.2 The Strengths of The Nascent Vortices

The vortex shedding is associated with boundary layer separation. The strengths of nascent vortices can then be estimated by analysing the boundary layer vorticity flux at the separation point. Fig.3 shows a typical boundary layer diagram in which U_s is the speed of the main stream just outside the boundary layer. The vorticity can be written as

$$\Omega = \frac{\partial v}{\partial x} - \frac{\partial u}{\partial y}$$

We assume that the vortex shedding rate equals to the boundary layer's vorticity flux, i.e.

$$\frac{\Delta \Gamma}{\Delta t} = \int_0^{\delta} \Omega \, u \, dy = -\frac{1}{2} U_s^2 \qquad (7)$$

This relationship was proved to be a close estimate of the vorticity fed into the vortex sheet (Fage, A. & Johansen, F. C. (1928)) and has been used by other authors (Clements, R. R. (1973), Sarpkaya, T. (1975), Sarpkaya, T. & Schoaff, R. (1979)).

Once the main stream speed U_s is known, we can work out the nascent vortex strengths quite easily from equation (7). If there is one nascent vortex shed from the

body surface in every k time steps, its strength is then

$$\Gamma = -\frac{1}{2} U_s^2 \, k \, \Delta t \tag{8}$$

In our inviscid model, the boundary layer thickness is neglected, and U_s is the transverse speed due to cross flow, the influence of longitudinal flow and free vortices effect. It is also assumed that, subsequent to their formation, the strengths of free vortices, i.e. those shed off from the body, do not change with time.

4.3 The Velocity Potential Induced by The Body

There are various approaches to determine the potential due to a body in a 2-D flow field. In the present study, the body is represented by a number of discrete vortices--also called bound vortices since they are attached to the body surface. By applying the body boundary condition, the vortices' strengths can be determined and hence the potential. The main advantage of this method over conformal mapping is its suitability to general body geometries. It is also more straight forward mathematically since it solves the problem on the physical plane only without involving parametric planes.

Assuming the speed of incoming flow is U and the body is stationary, the complex potential W at any instant t can be written as

$$W(z,t) = U\, z - \sum_{n=1}^{N} \frac{i\Gamma_{bn}}{2\pi} \ln(z - z_{bn}) + W_f \tag{9}$$

in which
N is the number of discrete vortices representing the body,
Γ_{bn} is the strength of nth bound vortex,
$z_{bn} = x_{bn} + iy_{bn}$ is the position of the nth bound vortex,
$W_f(z,t)$ is the complex potential of free vortices

$$W_f(z,t) = -\sum_{m=1}^{M} \frac{i\Gamma_{fm}}{2\pi} \ln(z - z_{fm})$$

where Γ_{fm} is the strength of the mth free vortex and z_{fm} is its position.

Note that $W_f(z\ ,\ t)$ is a known quantity since Γ_{fm} is decided by equation (6), and z_{fm} is determined by following the convection of the free vortices using

$$z_{fm}(t) = z_{fm}(t - \Delta t) + \overline{\left(\frac{dW}{dz}\right)}_{t - \Delta t} \Delta t$$

To determine the strengths of bound vortices, we apply the boundary condition to the body surface

$$\vec{V}\, n_b = u\, n_x + v\, n_y = 0 \tag{10}$$

where (u,v) is the flow speed and $(n_x,\ n_y)$ is the unit normal to the body surface.

Using $u = \mathrm{Re}\,(\frac{dW}{dz})$, $v = -\,\mathrm{Im}\,(\frac{dW}{dz})$ and expression (9), the equation (10) can be written as a set of linear equations from which the strengths of bound vortices can be determined

$$\sum_{n=1}^{N} \Gamma_{bn}\, A_{nj} = C_j \qquad j = 1,\ 2,\ \cdots\ ,\ N \tag{11}$$

in which A_{nj} andC_j are all known quantities and are defined as

$$A_{nj} = \frac{1}{2\pi}\,\frac{-(y_j - y_{bn})\, n_{xj} + (x_j - x_{bn})\, n_{yj}}{(x_j - x_{bn})^2 + (y_j - y_{bn})^2}$$

$$C_j = -\,U\, n_{xj} - \frac{1}{2\pi}\sum_{m=1}^{M} \Gamma_{fm}\,\frac{(y_j - y_{fm})\, n_{xj} + (x_j - x_{fm})\, n_{yj}}{(x_j - x_{fm})^2 + (y_j - y_{fm})^2}$$

and $(x_j,\ y_j)$ is the point on the body surface at which the boundary condition is applied. In the present calculation, we chose a point in the middle of each body surface element

$$x_j = 0.5\,(x_{b\,j+1} + x_{bj})\ , \quad y_j = 0.5\,(y_{b\,j+1} + y_{bj})$$

Once the bound vortices strengths Γ_{bn} are determined, the complex potential W(z,t) in expression (9) becomes a known function and can be used to calculate the forces on the body using Blasius formula

$$D - iL = i\frac{\rho}{2}\int_c \left[\frac{dW}{dz}\right]^2 dz + i\rho\frac{\partial}{\partial t}\int_c \overline{W}\, d\,\overline{z}$$

in which D and L are drag and lift respectively.

In the present notation the above integrals yield (Stansby, P.K. 1981)

$$D = -\rho \frac{\partial}{\partial t}\left(\sum_{m=1}^{M} \Gamma_{fm}\, y_{fm} + \sum_{n=1}^{N} \Gamma_{bn}\, y_{bn} \right) \tag{12a}$$

$$L = \rho \frac{\partial}{\partial t}\left(\sum_{m=1}^{M} \Gamma_{fm}\, x_{fm} + \sum_{n=1}^{N} \Gamma_{bn}\, x_{bn} \right) \tag{12b}$$

4.4 Some Computation Results

In the computation of the vortices shedding and convection in the wake using the model discussed above, it was found that by introducing a small separation angle, i.e. the angle between the nascent vortex velocity and the tangent of the body surface at separation point, the stability of the vortex sheets and the drag force could be improved without causing significant difference to the computation results. Computations were conducted for both without and with artificial disturbances. In the later case, disturbances were applied, at early stage of vortex shedding, to the vortex sheets by doubling the strengths of two vortices in one of the two vortex sheets. In order to prevent singular behaviour from occuring, the distance between any two vortices was checked at each time step. If two vortices were found to be too close to each other, they would be merged into one whose strength and location would be determined by

$$\Gamma_{new} = \Gamma_1 + \Gamma_2$$

and

$$z_{new} = \frac{|\Gamma_1|\, z_1 + |\Gamma_2|\, z_2}{|\Gamma_1| + |\Gamma_2|}$$

Fig.4 shows the vortex system, without artificial disturbance, behind a circular cylinder at different stage in the time history. Some asymmetries can be seen between the two vortex sheets, especially at later time stage, which are caused by the accumulation of numerical errors in the computation. The calculated time history of drag force are given in Fig.5 and Fig.6. The effect of separation angle, i.e. the angle between the nascent vortex velocity and the body surface tangent, is shown in Fig.5a, which indicates very limited influence on the drag force. The drag forces calculated with different time step sizes are given in Fig.5b. It shows that at early time stage, the two curves corresponding to different step sizes have quite significant difference, but they converge to the same level as time increases. It can also be seen that the oscillation in drag force occurs earlier when the time step is smaller. The curve in Fig.6 is the drag force time history up to tU/R=30. The step size in the calculation is 0.2. The drag descends with the time until about tU/R=13 and then levels off at about Cd=1.0. There are some sharp peaks in the curves which might be caused by certain irregular moves of vortices.

The results shown in Fig.7 and Fig.8 are for a circular cylinder with an disturbance

applied to the vortex system at tU/R=1.0. Although no further disturbance is applied, the distortion in the vortex system caused by the initial disturbance develops with the time and eventually the wake becomes a oscillating vortex street as can be seen in Fig.7. Similar result was also obtained by other researchers (Sarpkaya, T. & Schoaff, R. (1979), Stansby, P. K. (1981)).

Although the vortex shedding from a circular cylinder has also been studied by other researchers, the method presented in this report is applicable to general body geometries. As an example, calculations were carried out for an ellipse of b/a=10 and the results are given in Fig.9 and Fig.10.

5. A SOURCE ELEMENT METHOD TO CALCULATE THE VELOCITY AROUND THE HULL DUE TO LONGITUDINAL FLOW

In the previous section a two dimensional vortex shedding model was presented which could be used to calculate the forces on a section of a 3-D hull due to cross flow. In order to extend this method to calculate the side forces on a three dimensional slender body, the effect of longitudinal flow, which is the major difference between 2-D and 3-D problems, should be taken into account. In this section, a source element method is to be discussed which was adopted to calculate the velocity distribution on and around a slender body surface in an incoming flow without incidence. As an example, stream lines on "Mariner" hull and "British Bombardier" hull were calculated. It should be noted that, for the symmetric case of a hull at zero heel angle, the longitudinal flow potential ϕ_1 does not contribute directly to the side force or yaw moment on a hull, as is indicated in expression (2). However it does effect the flow velocity on the hull as can be seen in Fig.14 and Fig.15, which in turn will influence the strengths of the shedding vortices and their positions, and therefore influence the force and moment. If the hull is heeled the flow becomes asymmetric and a yaw moment will be introduced by ϕ_1.

5.1 Distributed Source Element Method

Assume ϕ is the potential of disturbance from a slender body to the main stream of speed U without incidence, after omitting high order small quantities, the body boundary condition requires:

$$\phi_x n_x + \phi_y n_y = u n_x + v n_y = - U n_s \qquad (13)$$

in which n_x, n_y, n_s are the components of the unit normal of the body surface.

Equation (13) suggests that for a slender body, the 3-D problem can be approximated by a number of sectional 2-D problems. In the present approach, the body section is represented by a number of source elements of constant strength. For a source element as shown in Fig.11, the induced velocity components at a point P(x,y) can be

expressed as:

$$v_\tau = \frac{q}{2\pi} \ln\frac{d1}{d2} \tag{14a}$$

$$v_n = \frac{q}{2\pi} \operatorname{sgn}(\vec{d1}\ \vec{n})\ \theta \tag{14b}$$

where q is the source strength of the element, d1 and d2 are the distances from the ends of the element to P(x,y), and θ is the angle between $\vec{d1}$ and $\vec{d2}$.

Using (14a) and (14b), u,v can be expressed as:

$$u = v_\tau\, n_y + v_n\, n_x \tag{15a}$$

$$v = -\, v_\tau\, n_x + v_n\, n_y \tag{15b}$$

Assume a section is represented by N elements, the boundary condition (13) can then be written as:

$$\sum_{k=1}^{N} q_k\, A_{kj} = B_j\,, \qquad j = 1,\ \cdots\ ,N \tag{16}$$

in which q_k is the source strength of kth element

$$A_{k,j} = \frac{1}{2\pi}\ [\ (n_{xk}n_{xj} + n_{yk}n_{yj})\ \operatorname{sgn}(\vec{d1}_{kj}\ \vec{n_k})\ \theta_{kj} + (n_{yk}n_{xj} - n_{xk}n_{yj})\ \ln\frac{d1_{kj}}{d2_{kj}}\ ]$$

$$B_j = -\, U\, n_{sj}$$

The strengths of the source elements q_k (k=1,2,...,N) can now be determined by solving Equation (16). Using expression (14) or (15), the flow velocity induced by each source element can be calculated.

5.2 Sectional Interpolations

Sectional interpolations are sometimes necessary to increase the number of hull sections for the precision of the calculation. It was found to be more convenient to interpolate the mapping coefficients rather than the original offsets to increase the section number. The mapping method discussed in Section 3 was used to calculate the mapping coefficients for each original section. These coefficients were then used in the interpolation to calculate the coefficients for new sections. Once the mapping coefficients are known, the offsets for each section can be calculated using expression (5). Fig.12 shows the "Mariner" hull consists of 39 sections obtained by interpolating

the original 23 sections. The "British Bombardier" hull form given in Fig.13 has 49 sections, which was obtained from the original 26 sections through interpolation.

5.3 Calculated Streamlines

To validate the present method, computations were carried out for the "Mariner" hull and "British Bombardier" hull. It was assumed in the computations that the ships were moving forward at constant speed and zero drift angle.

The streamlines on the "Mariner" hull are plotted in Fig.14a (side view) and Fig.14b (bottom view). It can be seen that the flow converges towards the centreline in the bow area and diverges away from the centreline in the stern area. Similar pictures for the "British Bombardier" hull are given in Fig.15a and Fig.15b

It should be noted that the longitudinal flow does not contribute directly to the side force or yaw moment on a hull, which is indicated in expression (2). However it does effect the flow velocity on the hull as can be seen in Fig.14 and Fig.15, which in turn will influence the strengths of the shedding vortices and their positions, and thus influence the force and moment.

6. CALCULATION OF THE FORCES ON SLENDER SHIPS

6.1 . A 3-D Model for Calculating Vortex Sheets Convection

As we can see in the expression (2) that the sway force on the hull depends on the integral of the potential of the external vortex system which is determined by the strengths and locations of the free vortices. Differing from the 2-D case, the vortex shedding and vortices movement at a given section of a 3-D hull will be affected by other sections. On the ground that the ship is a slender body, we make the following assumptions to simplify the problem:

(1) Vortex shedding occurs at each section of the hull.
(2) A nascent vortex separates from the body surface at the point on the leeward side of the hull where the cross flow speed is the maximum. The cross flow speed referred to here does not include the effects of free vortices and longitudinal flow in order to achieve more consistent separation positions over the length of the hull for the sake of having more stable vortex sheets. This may cause some differneces to the separation position at some sections but is not expected to cause significant difference to the calculated forces.
(3) Free vortices travel downstream at the speed of the main stream, their velocities in the transverse plane are influenced only by the hull section and other free vortices in the same plane.
(4) The strengths of the free vortices are determined using the same method as

discussed before and they remain constant after leaving the body surface.

Besides the mainstream, the velocity of a free vortex in the present model is also decided by (a) cross flow effect represented by the bound vortices distributed on each hull section, (b) longitudinal flow effect represented by source distributions on each hull section, and (c) other free vortice's influence. In our calculation for the "Mariner" hull, 48 equally spaced sections were used which enabled us to use a uniform time step in the calculation over the whole length of the hull, i.e. it took the same length of time for a free vortex to travel from one section to the next section. The size of the time step was determined by the mainstream speed U and the section length Δs as

$$\Delta t = \Delta s/U$$

Due to the variation of the area and geometry of the hull section along the ship length in 3-D case, especially at those sections near the bow where the area increases quickly, the free vortices travelling from the upstream towards downstream can very easily go into the hull within a period of one time step. To avoid this, we recalculate the paths of those vortices found to be within the hull at the end of a time step by forcing them to move along the surface of the hull. Fig.16.a to Fig.16.d show the free vortex sheets at various sections of the "Mariner" hull. Note that in the present coordinate system as shown in Fig.1, the midships is at s=0. It can be seen that these sheets are not as regular as those we obtained in the 2-D computations. But they may not be unreasonable considering that the influence of source distribution on the movement of free vortices is found to be quite strong which causes the vortex sheet to migrate round the hull sections. The effect of the source distribution can also be seen in Fig.16a and Fig.16.b in which the vortex sheets move towards the keel over the forebody of the ship and move outwards over the afterbody. This phenomenon is consistent with the flow patterns generated by source distribution as presented in Fig.14. Calculation was also carried out for the "British Bombardier" hull and similar result was obtained as can be seen in Fig.17.

6.2 Calculation of Forces and The Results

In order to check whether the mathematical model presented in the above sections can provide a reasonable estimation of the sway force and yaw moment on a slender ship, calculations were conducted for the "Mariner" hull and "British Bombardier" hull in drifted forward motion at constant speed.

It can be seen in expression (2) that there are two contributors to the side force on a hull section: bound vortices and free vortices. The former represents the influence of the hull, and the latter represents the viscous effect. The total side force F on the whole ship can be obtained by integrating with respect to s in expression (3). Note that the section contours at both ends of the hull shrink to zero, there will be no contribution to F from the first integral in expression (3). In other words, the contribution to the net side force on a ship only comes from external free vortices as far as the present

approach is concerned. However, the first integral should not be neglected since it can have significant contribution to the moment.

The side force distributions along the "Mariner" hull at different drift angles are shown in Fig.18a and Fig.18b, in which the contributions from the bound vortices and free vortices were plotted separately. As we can see, the curves representing the bound vortices' contributions exhibit the typical properties of the potential flow about a non-lifting body. Although a vortex shedding process is introduced in the present approach, the shed free vortices do not appear to have significant influence on the side force or yaw moment generated by the bound vortices as can be seen in Fig.19. The comparisons of the calculated side force and yawing moment with the PMM test results are given in Fig.20 and Fig.21. The calculated side force shows stronger non-linearity and is generally lower than the measurement especially at small drift angles. On the whole the agreement is reasonably good. Significant discrepancies can be found between the calculated and measured yawing moment. This is mainly caused by the unrealistic contribution from the bound vortices to the moment, as is indicated in Fig.18. In the real flow, due to the influence of boundary layer, the curve of side force distribution will be much more flat in the aft ship area, and the yawing moment will consequently be reduced. Fig.22 shows the comparison of the calculated side force distribution with the segmented model measurement carried out by DRA Haslar. Besides the discrepancies caused by neglecting the boundary layer, the curves also show a pronounced difference in the bow area. The reason for the latter discrepancy is possibly that the lifting effect of the ship has not been taken into full account in the present approach. In fact, at small drift angles, the lifting effect can be at least as important to the side force as vortex shedding, and a high pressure area near the bow can be expected if the lifting effect is more appropriately considered. This may also account for the fact that the calculation generally underestimated the side force especially when the drift angle was small.

To investigate the influence of the lifting effect on the side force distribution, an attempt was made to calculate the hull's contribution to the side force distribution using a computation code based on the panel method. This code was written by Dr. S. Turnock of Ship Science Department, Southampton University, in which the ship was treated as a lifting body by imposing the Kutta condition at the stern, and the flow was purely potential without considering the free vortices. Since it has been found that the free vortices have quite limited influence on the side force and yaw moment caused by the hull, we expect that ignoring the interation between the hull and the free vortices in the panel method will not cause significant difference to the calculation result. The vortex shedding model, together with source element and bound vortices methods, were used for calculating the side force caused by free vortices. As can be seen in Fig.23, the side force distribution on the "Mariner" hull predicted by the panel method shows a peak in the bow area, which is typical for a thin lifting body. However, the panel method failed to predict the positive side force in the area near the stern, which may largely be due to neglecting the boundary layer effect which is more pronounced in the stern area. On the other hand, one can see in Fig.24 that the vortex shedding

method predicted all positive side force along the hull, and a high side force area near the stern. By adding together the side force distributions predicted by vortex shedding and panel method, the total side force distribution can be obtained. Fig.25 shows that except in the bow area this total side force distribution agrees quite satisfactorily with that measured in the segmented model test. Consequently, the agreement between the calculated and measured sway force and yaw moment is also improved as shown in Fig.26 and Fig.27.

Calculations were also carried out for the "British Bombardier" hull using the vortex shedding and bound vortice method. Fig.28 shows the calculated free vortices' and bound vortices' contributions to the side force distribution over the hull. It is interesting to see in Fig.29 a good consistency of the calculated side force distribution with the segmented model measurement (D. Clarke & G. E. Hearn, 1992) over most of the hull length except near the stern. The reason for the good agreement in the bow area can be explained using expression (2) which suggests that the higher change rate of the section area generally results in larger local side force. The "British Bombardier" hull is relatively a blunt body, as shown in Fig.13, whose section area increases quickly near the bow, which leads to higher side force in that area. On the other hand, the "Mariner" hull has a slower change rate of the section area near the bow and therefore no high local side force is predicted there. The calculated sway force and yaw moment are shown in Fig.30 and Fig.31 in comparison with the present PMM measurement. The calculated side force shows a reasonable agreement with the PMM measurement, but great discrepancy can be seen for the yaw moment. The large negative side force near the stern as shown in Fig.28, may explain the reason for the calculated yaw moment being too high. With the previous experience, it was expected that by applying the present vortex shedding model together with the panel method to the "British Bombardier" hull, better calculation results may be achieved for both side force and yaw moment. But due to the limit of time, this work was not carried out.

7. CONCLUDING REMARKS

In the present study a vortex shedding method has been developed for the estimation of the sway force and yaw moment on a slender ship. Source elements and bound vortices were also used to calculate the flow velocity caused by the presence of the ship hull. Numerical computations were conducted for the "Mariner" hull and "British Bombardier" hull. It was found that the calculated sway force had fairly good agreement with the PMM measurement, but the agreement between the calculated and measured yaw moments was not satisfactory. In the comparison of the side force distribution, a great deal of discrepancy was found between the calculation and the segmented model measurement for the "Mariner" hull. However when the ship was treated as a lifting body by using a panel method in place of the bound vortices method, much better calculation results were achieved. The panel method was not used for the "British Bombardier" hull. The agreement between the calculated and measured force and moment is largely the same as in the case of the "Mariner" hull,

but better agreement was found in the side force distribution. From a study and comparison of the calculation results obtained so far, the following conclusions might be drawn which will hopefully cast some light on the reasons for the agreement and disagreement between the calculation and measurement:

(1) The local side force caused by the bound vortices is closely related to the change rate of the section area. The positive side force on the fore half of the hull and the negative side force on the aft half of the hull is a direct result of the side force's dependence on the area change rate. The results indicate that the present bound vortices method tends to overestimate the side force caused by the area change rate.

(2) The lifting effect has a noticeable effect on the side force and yaw moment on the hull, which was not appropriately taken into account in the present method.

(3) The panel method which treats the hull as a lifting body can provide a better prediction of the side force distribution than the bound vortices method. However the panel method base on the pure potential theory is still unable to predict a realistic pattern of the side force distribution in the area near the stern, mainly due to the neglect of the boundary layer effect.

(4) The present vortex shedding model takes into account the vortex shedding from the hull, which is associated with the boundary separation, and predicts positive side force in the stern area. In this sense, the vortex shedding method and the panel method are complementary to each other, and reasonable calculation results can be expected when they are used together.

REFERENCES

Clarke, D. and Hearn, G. E. 1992
A Re–analysis of The Segmented Model Data for *The British Bombardier* and *Mariner Hullforms*
Report of MOSES Project

Clements, R. R. 1973
An Inviscid Model of 2–D Vortex Shedding
Journal of Fluid Mechanics, Vol.57, 1973, pp.321-336

Fage, A. & Johansen, F. C. 1928
The Structure of The Vortex Sheet
Phil. Mag., Vol.7, 1928, pp. 417-436

Kerczek, C and Tuck, E. O. 1969
The Representation of Ship Hulls by Conformal Mapping Functions
Journal of Ship Research, Vol.13, No.4, pp.284-298

Sarpkaya, T. 1975
An Inviscid Model of 2–D Vortex Shedding for *Transient* and *Asymptotically Steady Flow over An Inclined Plate*
Journal of Fluid Mechanics, vol.68, 1975, pp.109-128

Sarpkaya, T. and Schoaff, R. 1979
Inviscid Model of Two–Dimensional Vortex Shedding by a Circular Cylinder
AIAA Journal, No.11, November 1979, pp.1193-1200

Stansby, P. K. 1981
A Numerical Study of Vortex Shedding One and *Two Circular Cylinders*
Aeronautical Quarterly, Vol. 32, Feb. 1981, pp.48-64

Wellicome, J. F. 1981
Slender Body Theory Applied To Asymmetric Bodies Fitted with Lifting Appendages
Department Report, Department of Ship Science, University of Southampton

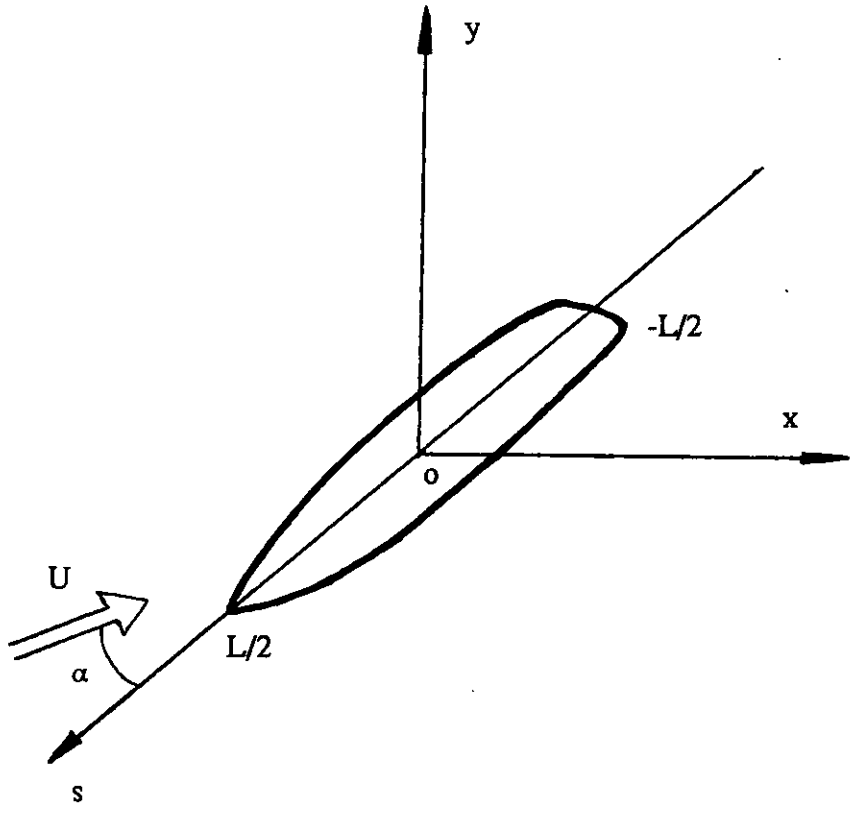

Fig.1 Coordinate System

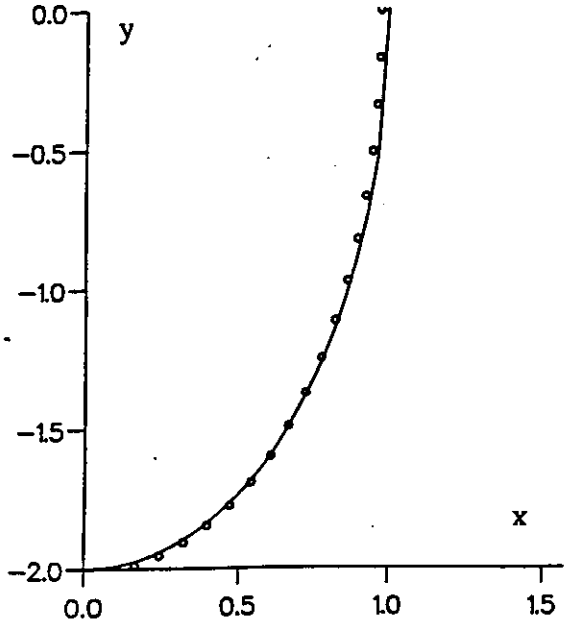

Fig. 2(a) Ellipse
o mapped from unit circle
– exact curve

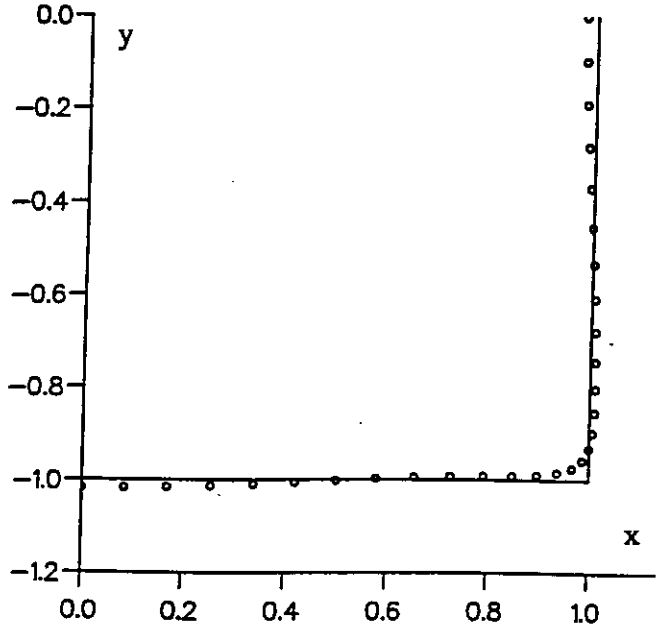

Fig. 2 (b) Square
o mapped from unit circle
- exact curve

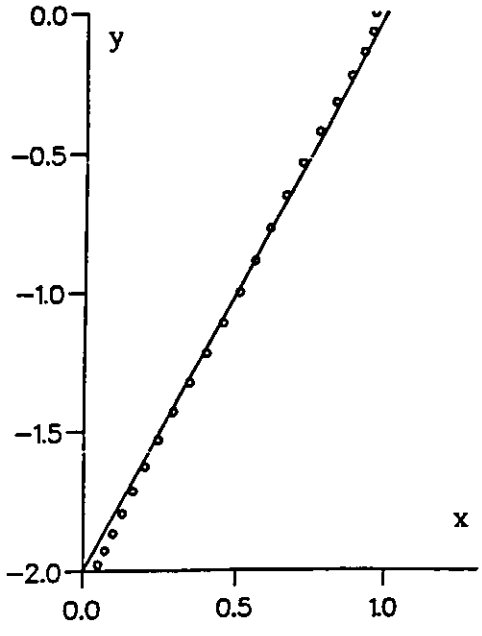

Fig. 2(c) Prismatic Hull
o mapped from unit circle
– exact curve

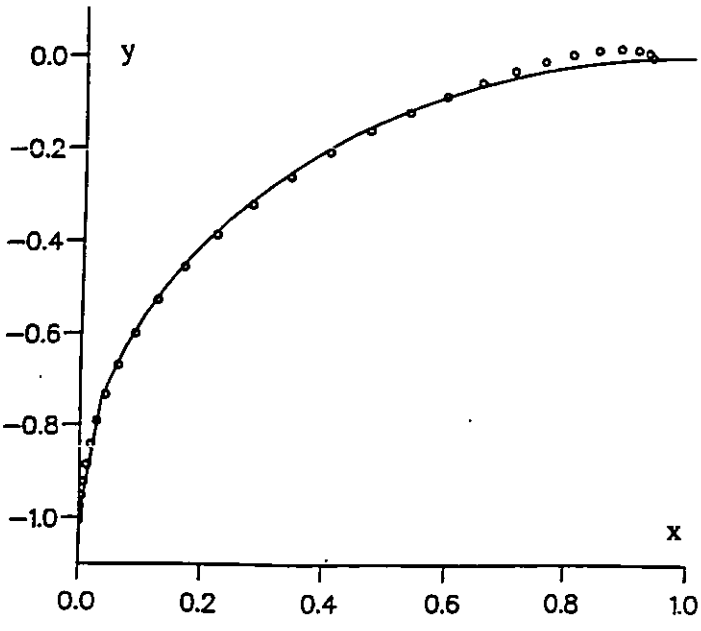

Fig. 2(d) Cusped Hull
o mapped from unit circle
– exact curve

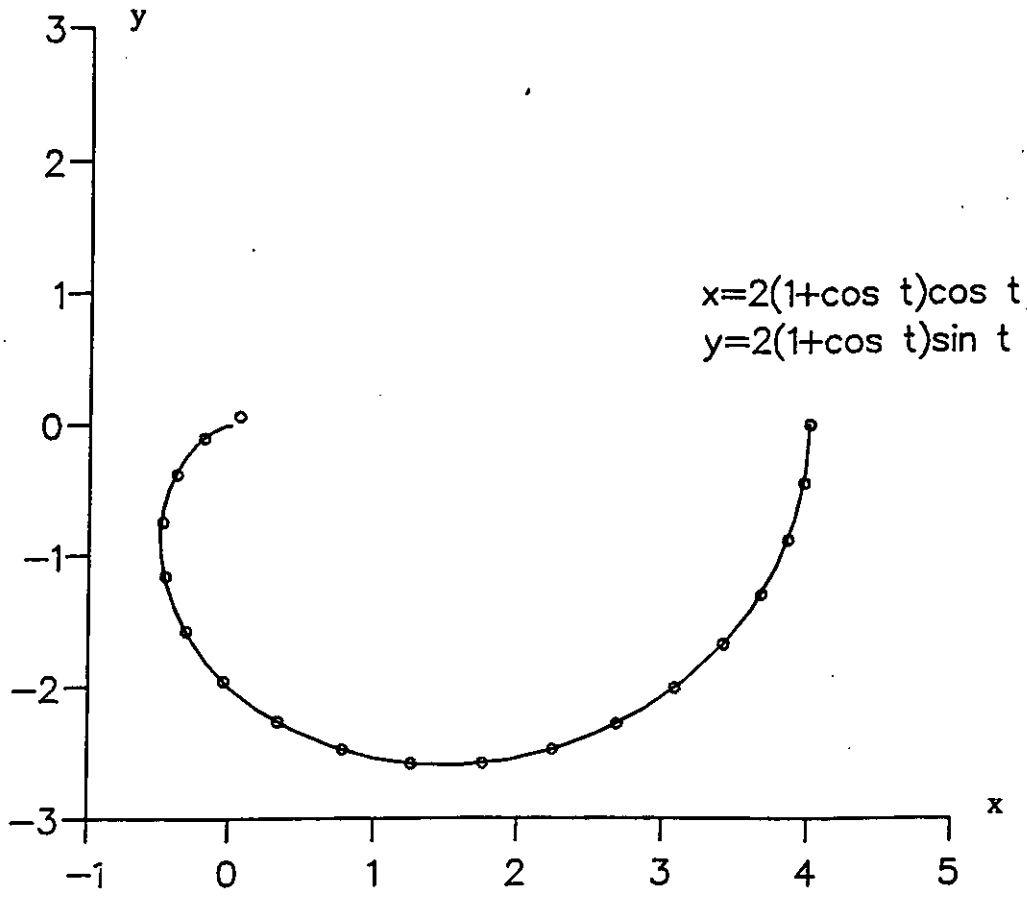

(e) Asymmetric Body

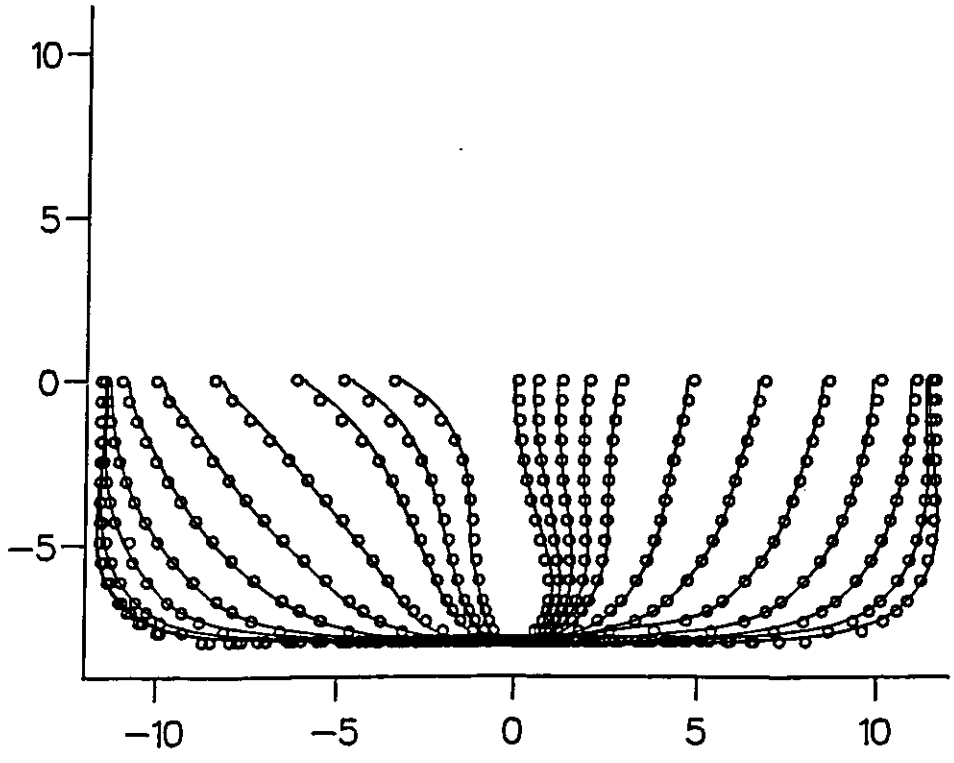

(f) Mariner Hullform

Fig.2 Some Examples of Conformal Mapping

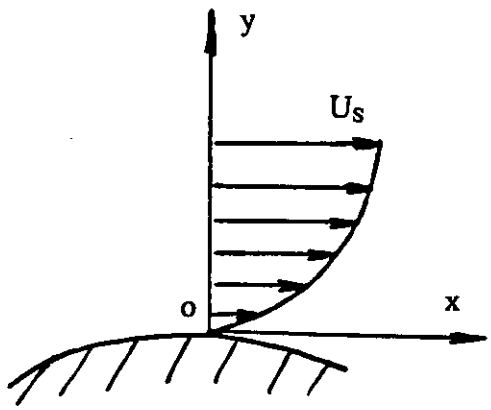

Fig.3 A Sketch of Boundary Layer

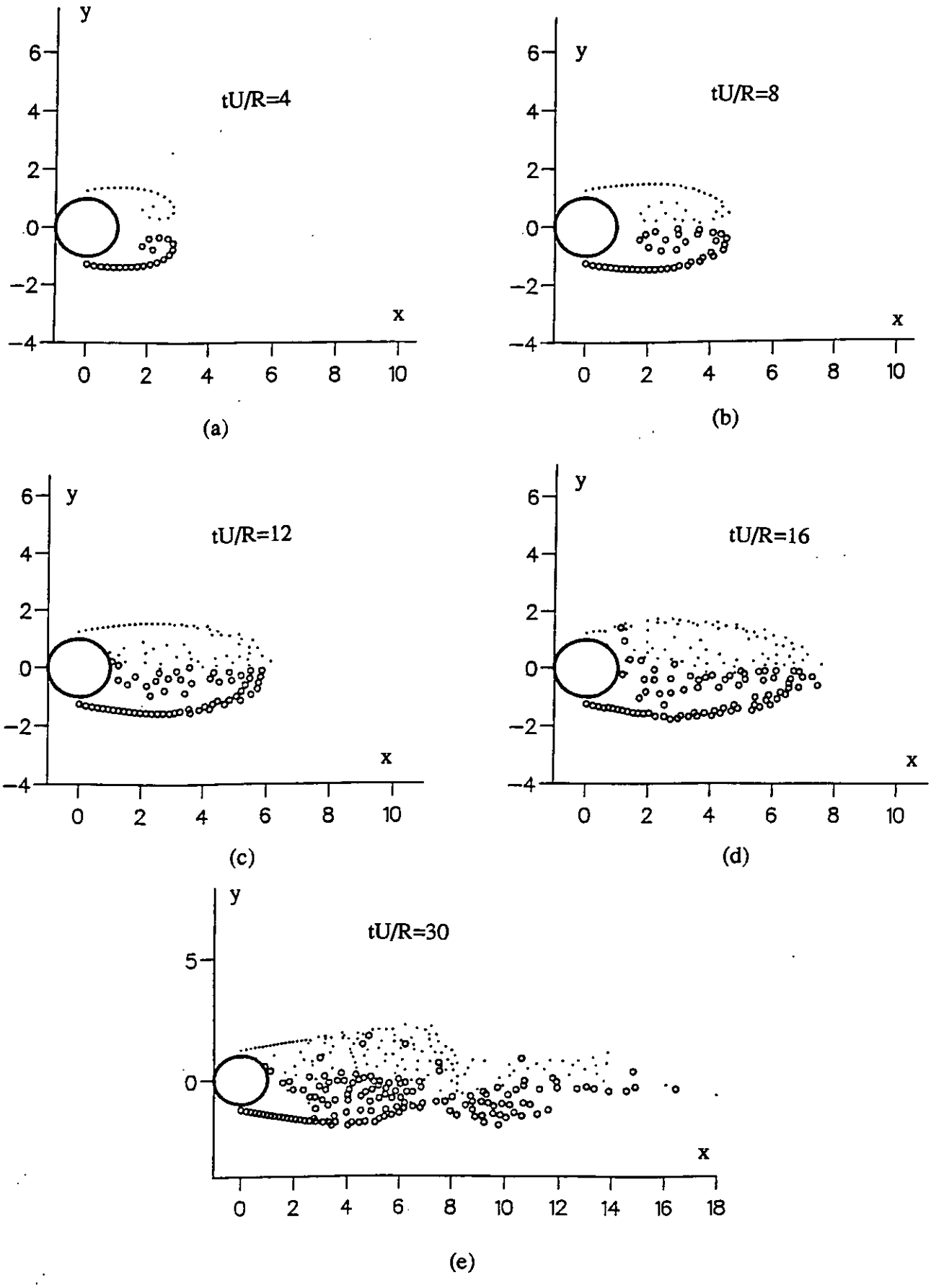

Fig.4 Vortex Sheets at Various Times without Applying Artificial Disturbance

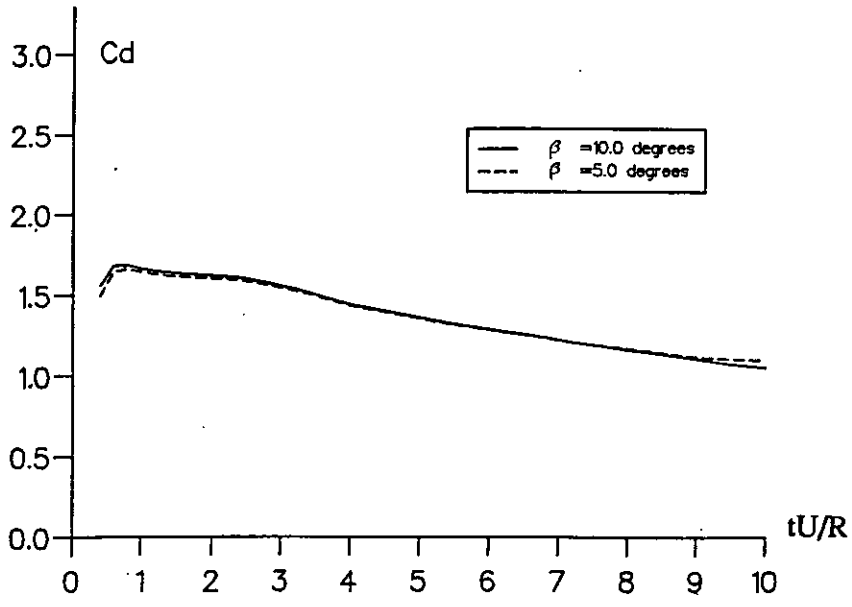

Fig.5(a) The Effect of Separation Angle β on The Drag Force
(β is defined as the angle between the velocity of the nascent vortex and the tangent of the body surface at the separation point)

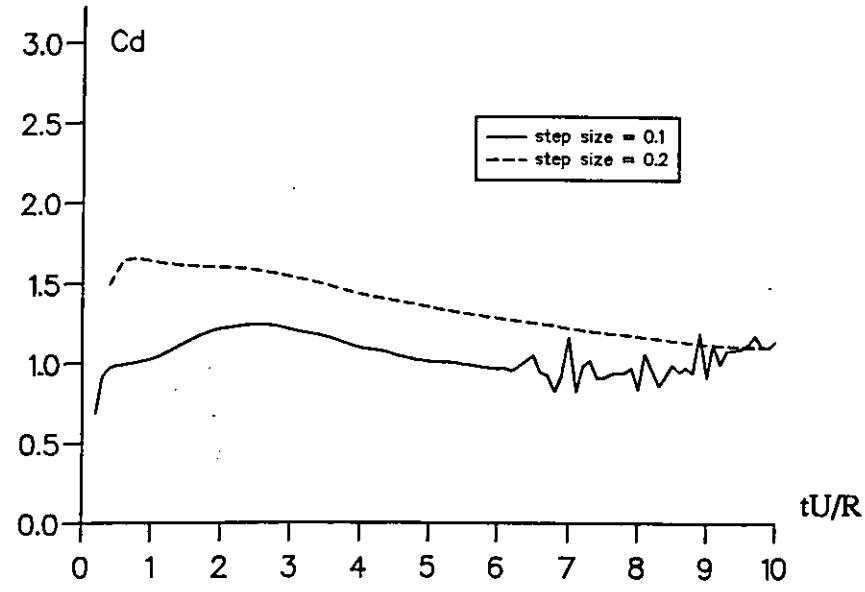

Fig.5(b) The Effect of The Step Size ΔtU/R on The Drag Force

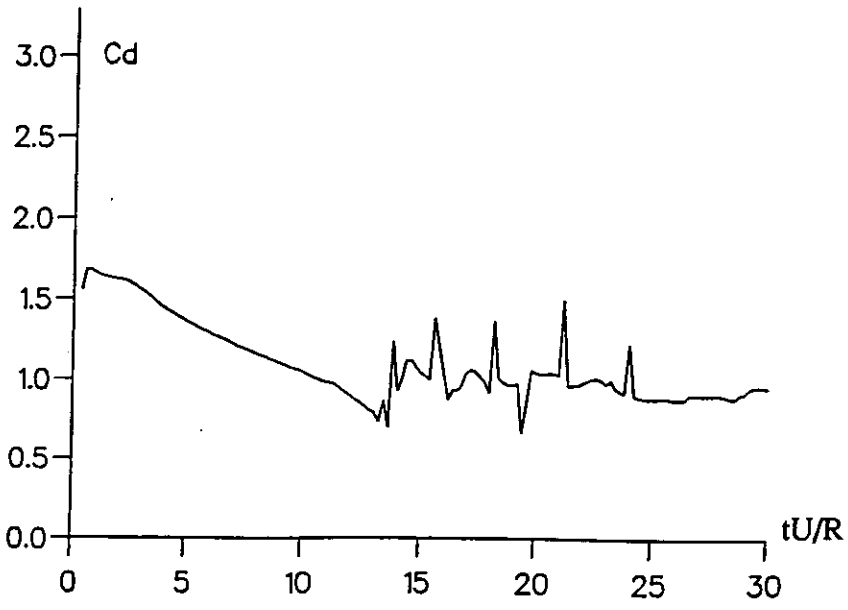

Fig.6 The Time History of The Drag Force on The Cylinder
(without artificial disturbance to the vortex sheets)

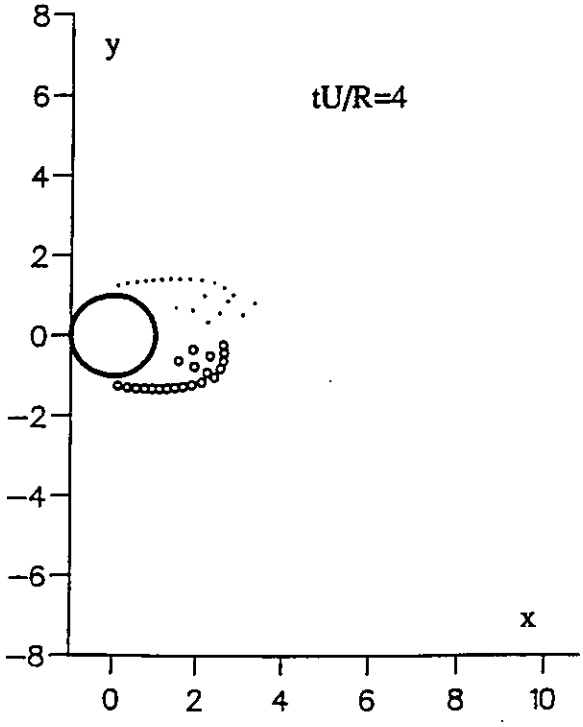

Fig.7 (a)

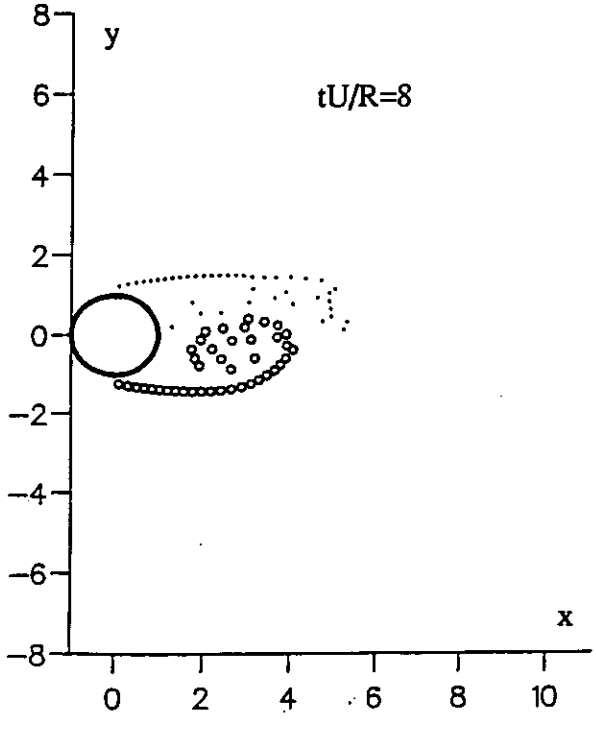

Fig.7 (b)

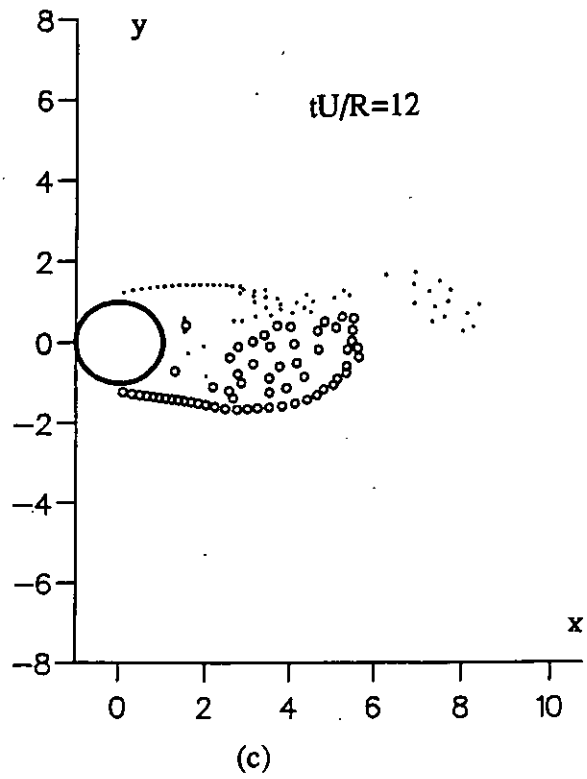

(c)

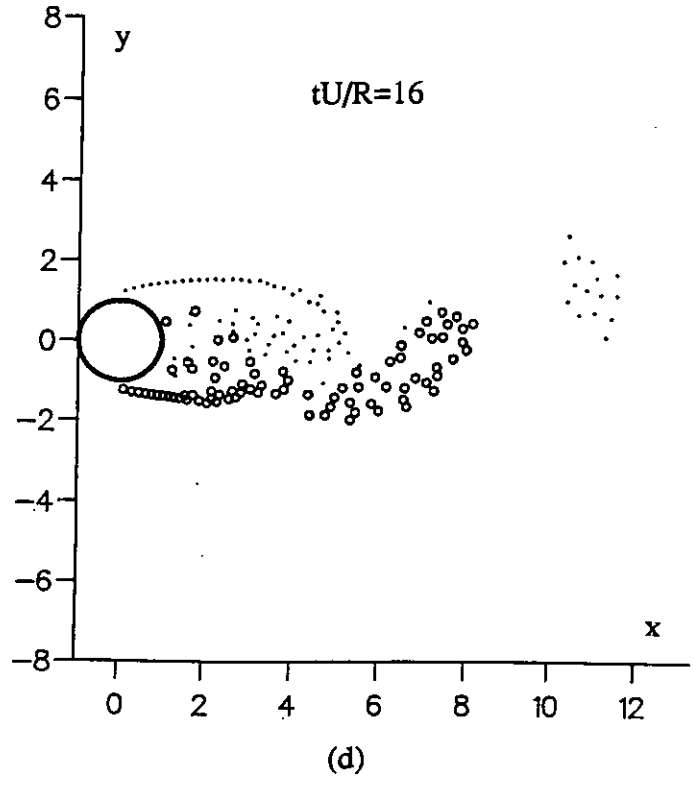

(d)

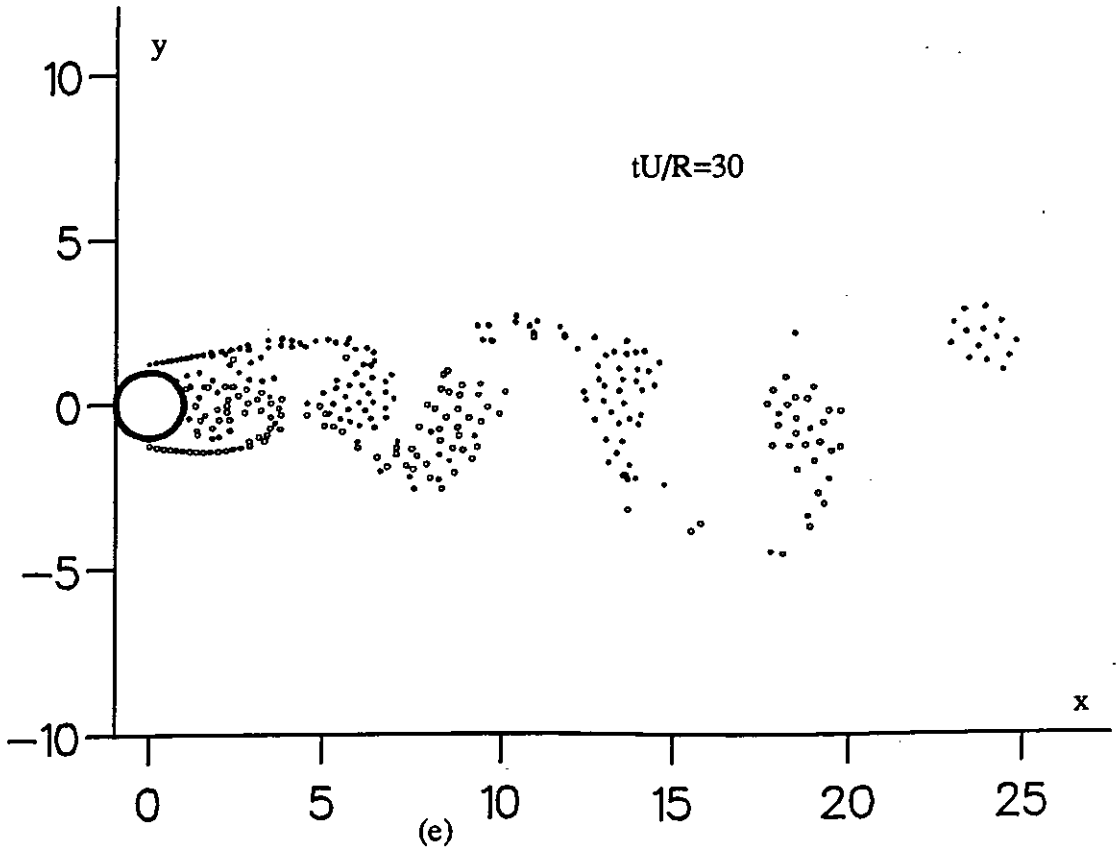

(e)

Fig.7 Vortex Sheets at Various Times with Artificial Disturbance

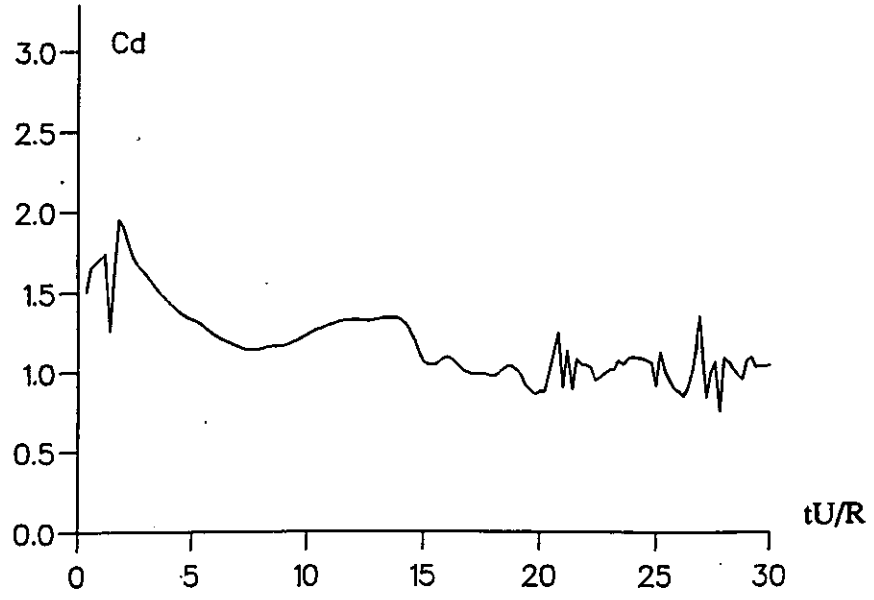

Fig.8 The Time History of The Drag Force on The Cylinder
(with artificial disturbance to the vortex sheets)

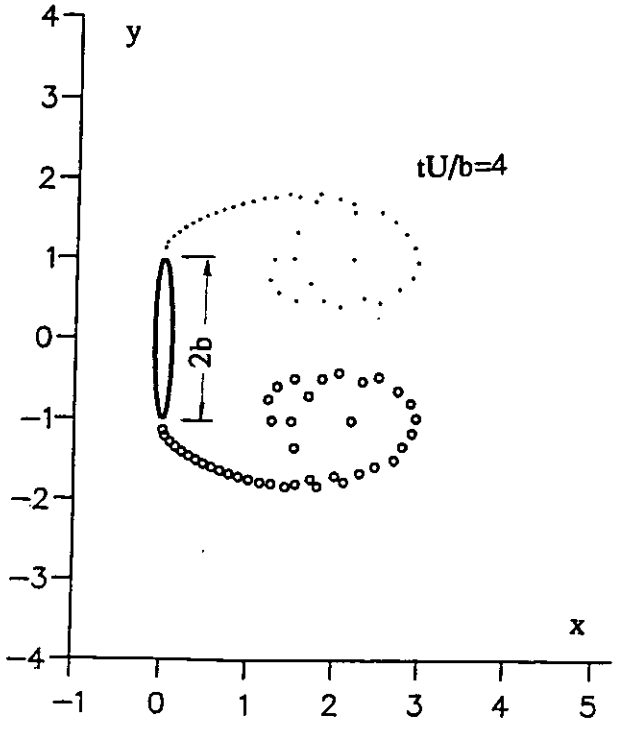

Fig.9 (a)

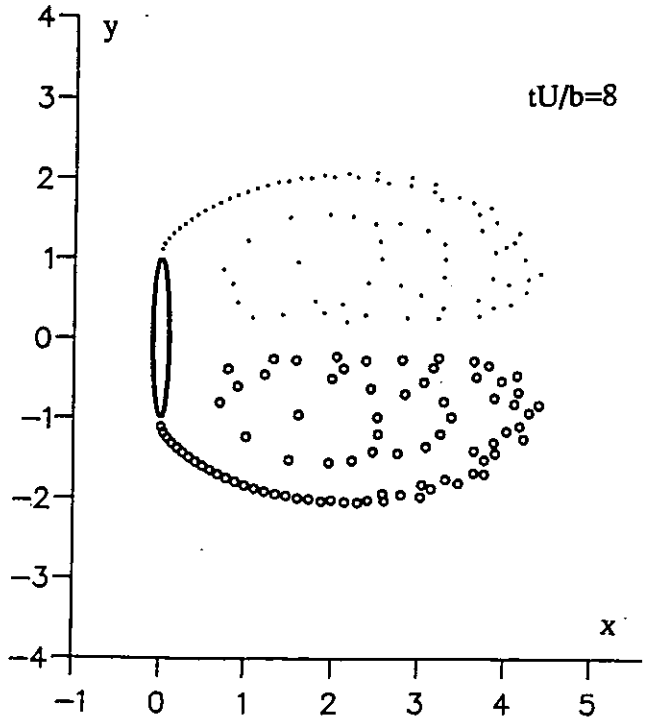

Fig.9 (b)

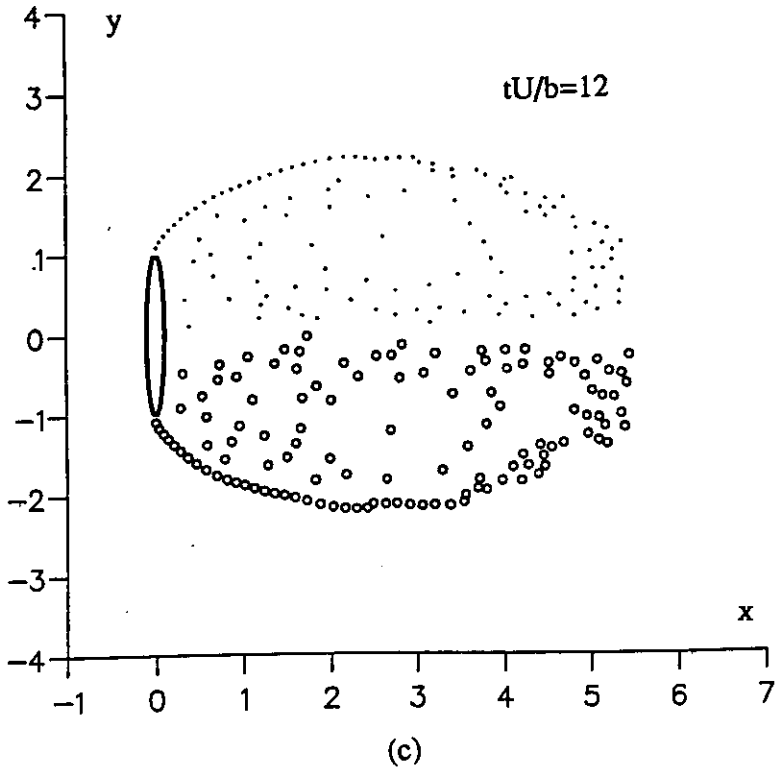

Fig.9 Vortex Sheets Shed from An Ellipse

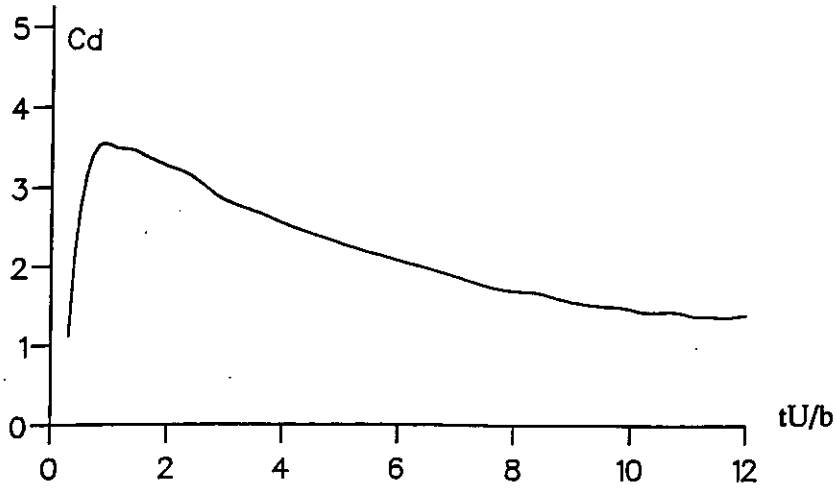

Fig.10 The Time History of The Drag Force on The Ellipse

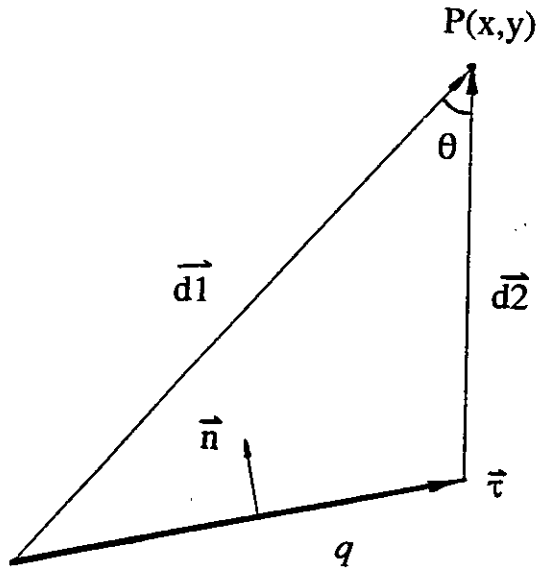

Fig.11 A Sketch of A Source Element

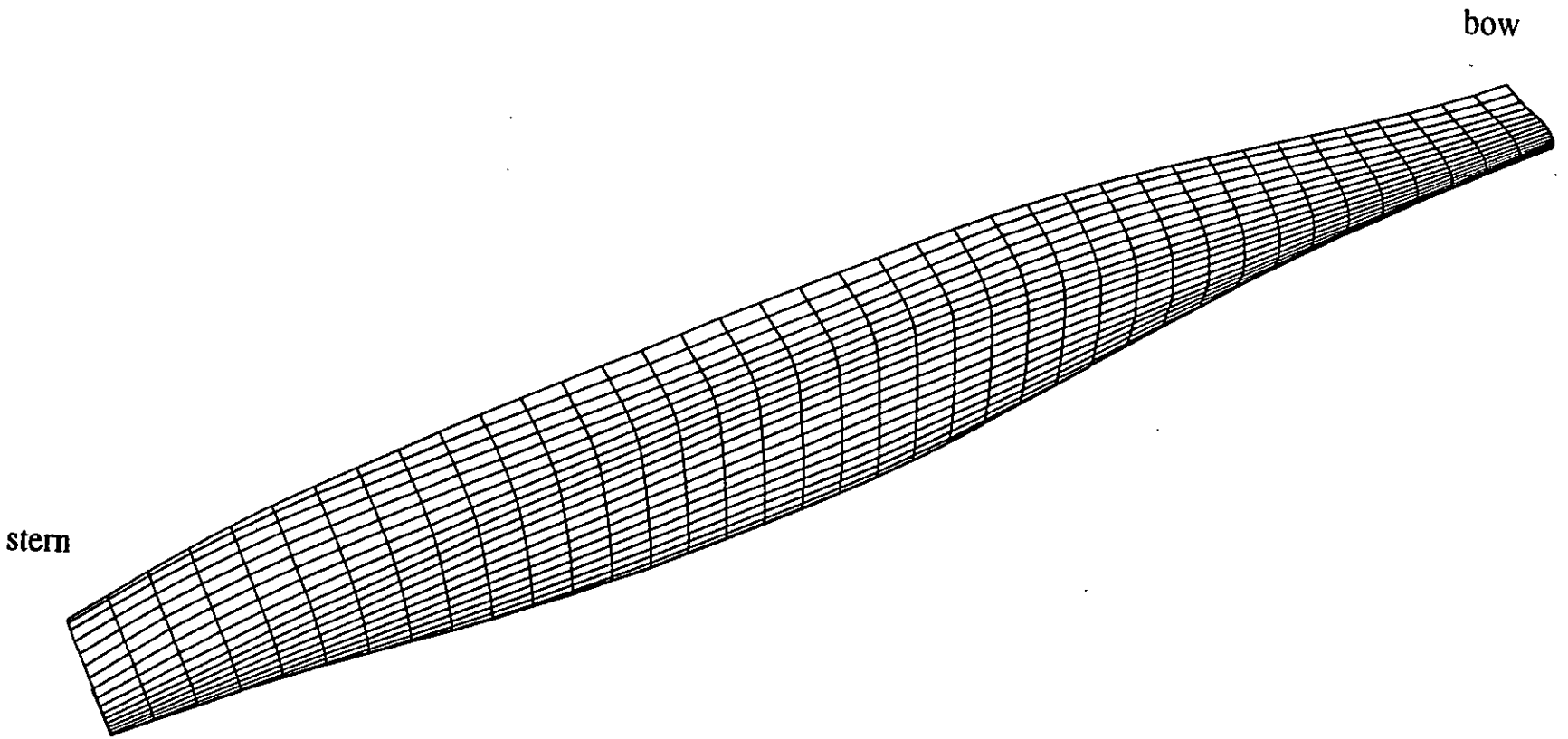

Fig.12 The Mariner Hullform Obtained from Sectional Interpolation

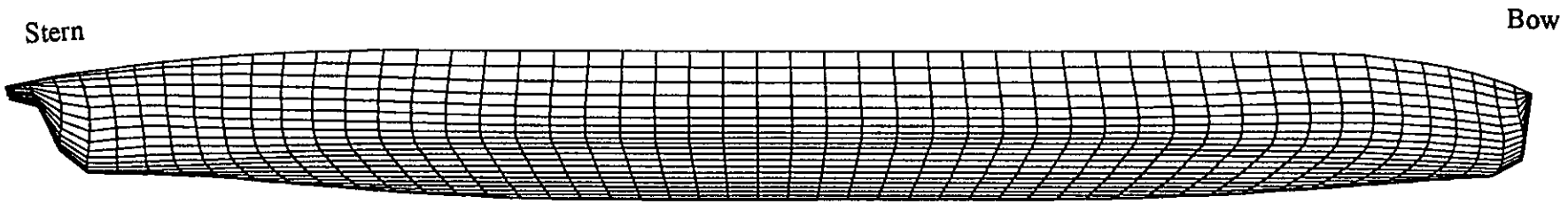

Fig.13 The British Bombardier Hullform Obtained from Sectional Interpolation

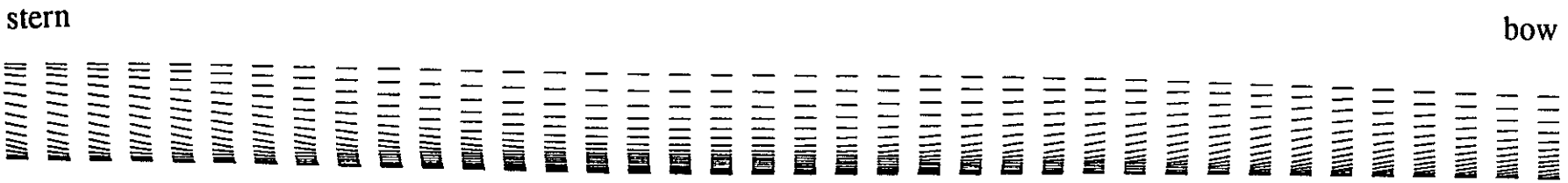

Fig.14(a) A Side-view of The Streamlines on The Mariner Hull

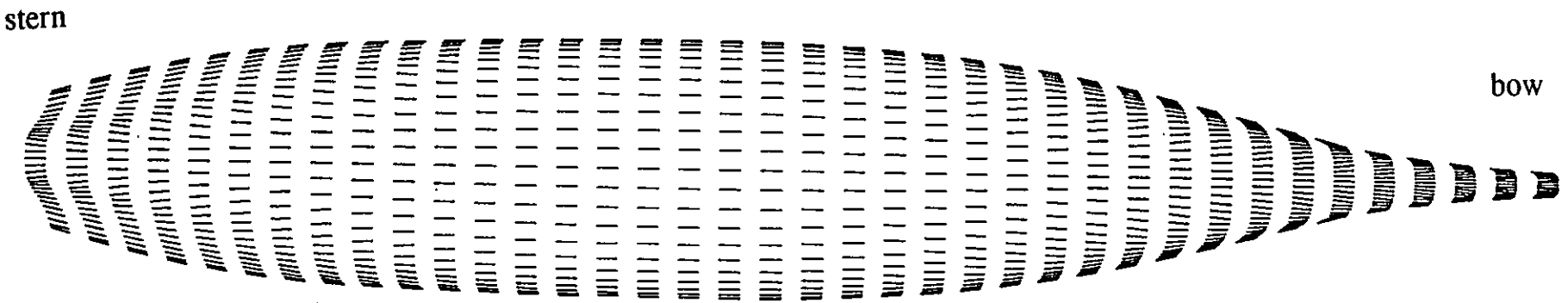

Fig.14(b) A Bottom-view of The Streamlines on The Mariner Hull

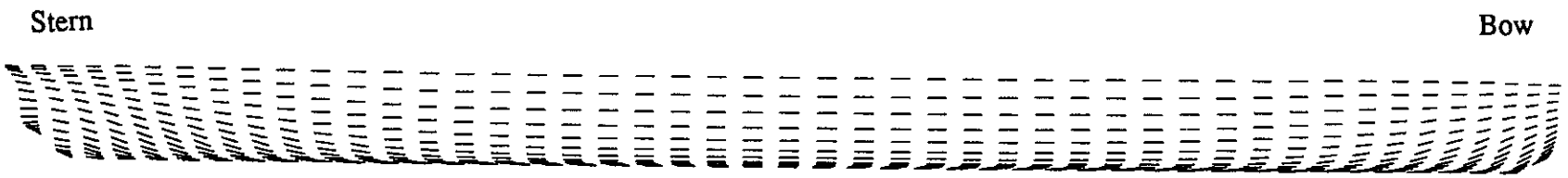

Fig.15(a) A Side-view of The Streamlines on The British Bombardier Hull

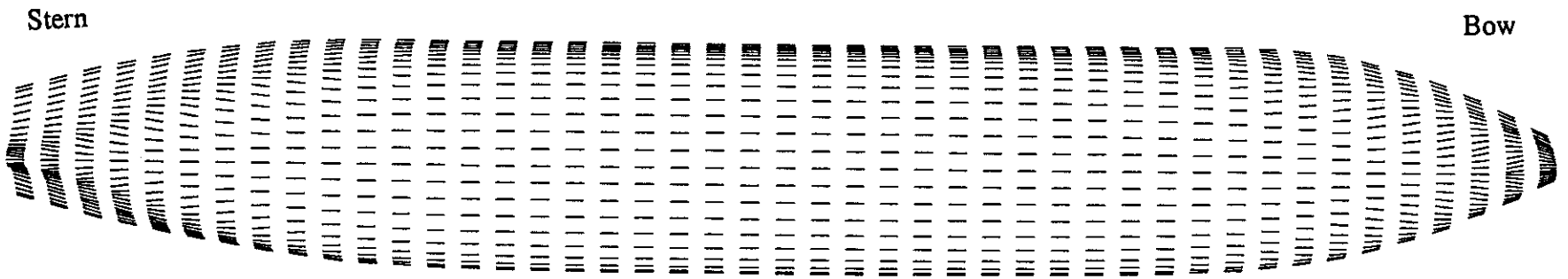

Fig.15(b) A Bottom-view of The Streamlines on The British Bombardier Hull

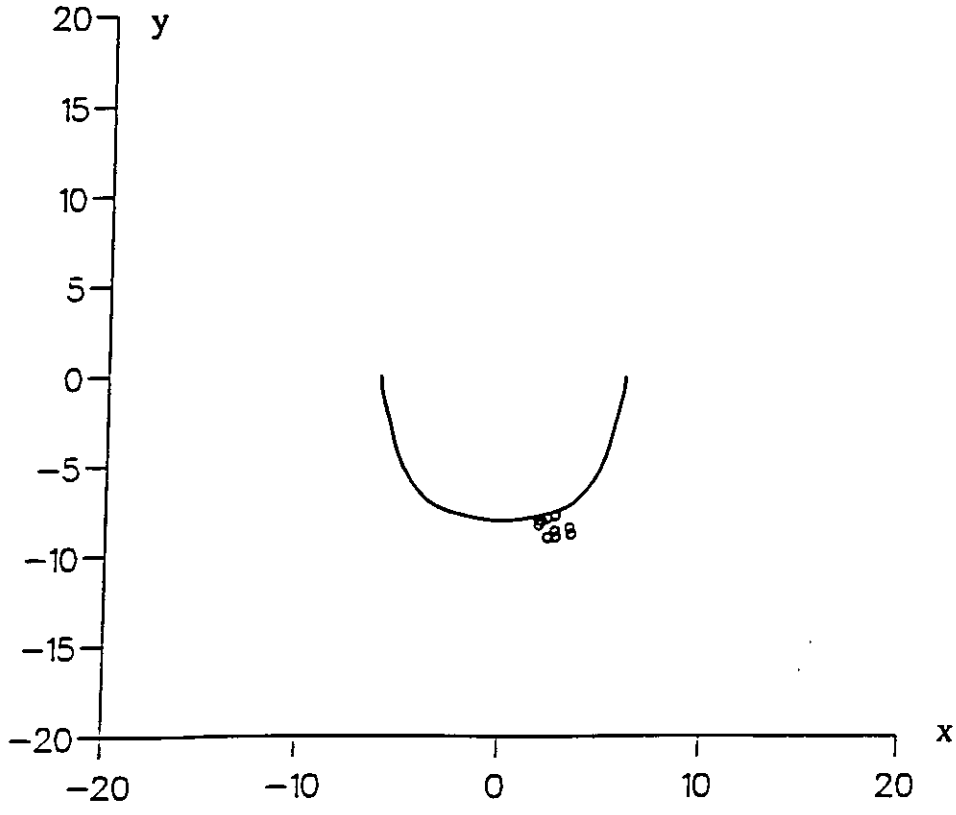

(a) Vortex Sheet at s=0.30L

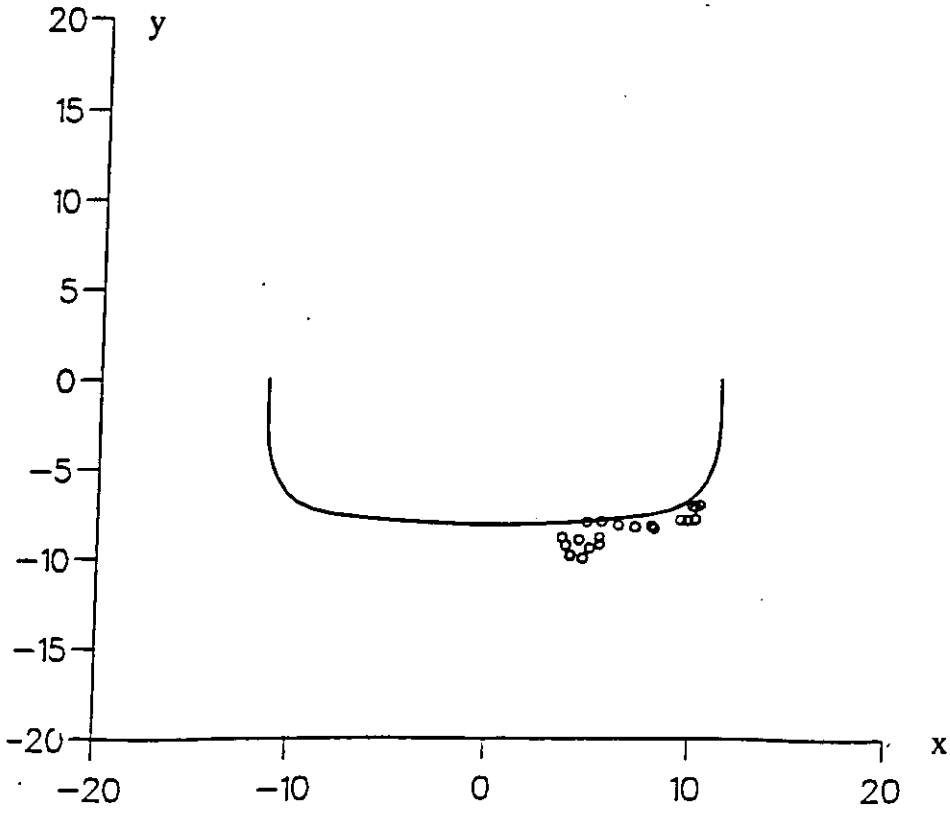

(b) Vortex Sheet at s=0.08L

Fig.16 Vortex Sheets at Various Sections on the Mariner Hull
(drift angle=4.0 degs.)

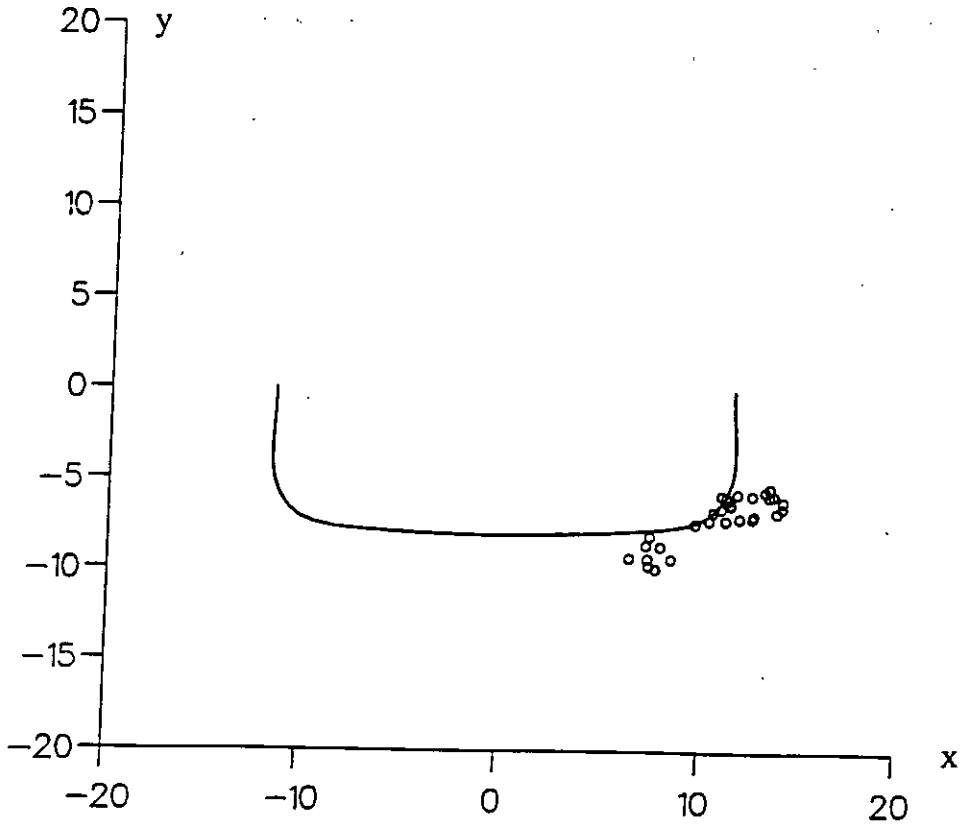

(c) Vortex Sheet at s=-0.14L

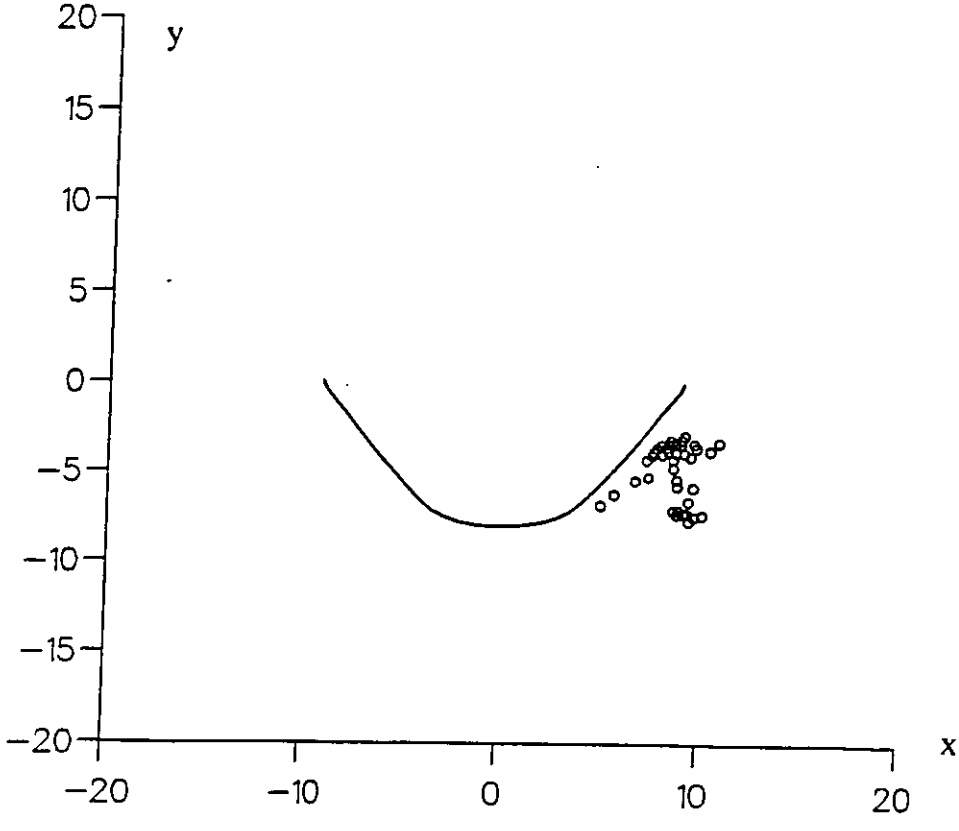

(d) Vortex Sheet at s=-0.35L

Fig.16 Vortex Sheets at Various Sections on The Mariner Hull
(drift angle=4.0 degs.)

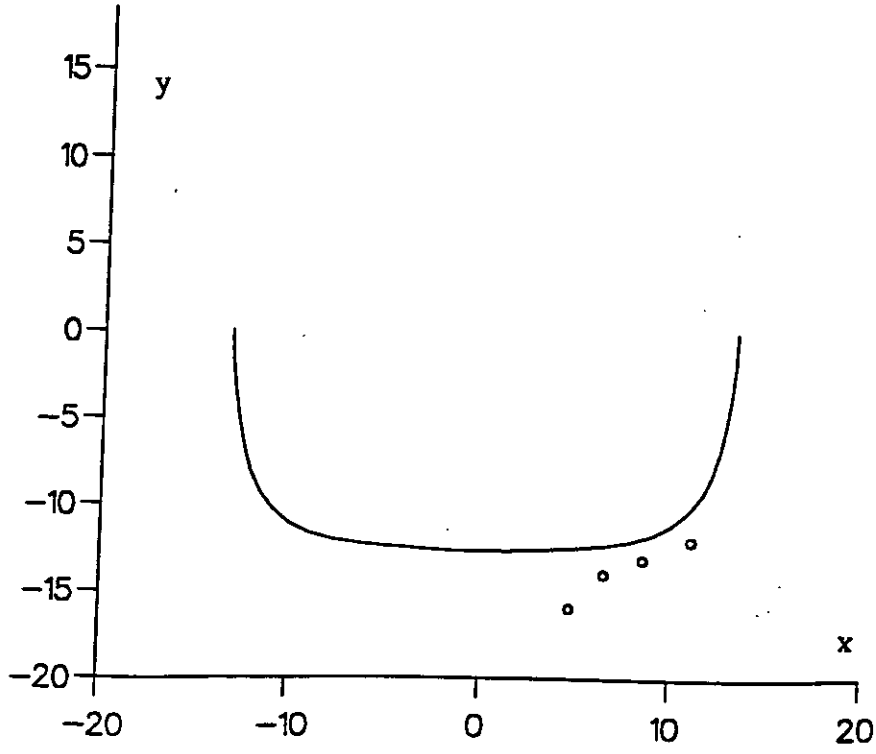

(a) Vortex Sheet at s=0.36L

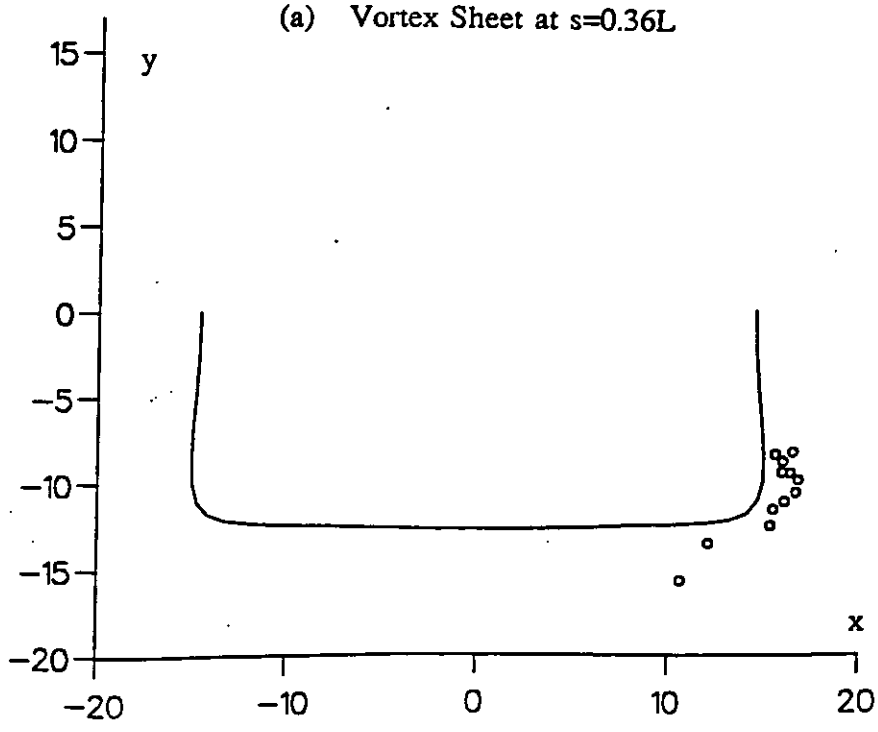

(b) Vortex Sheet at s=0.06L

Fig.17 Vortex Sheets at Various Sections on the British Bombardier Hull (drift angle=4.0 degs.)

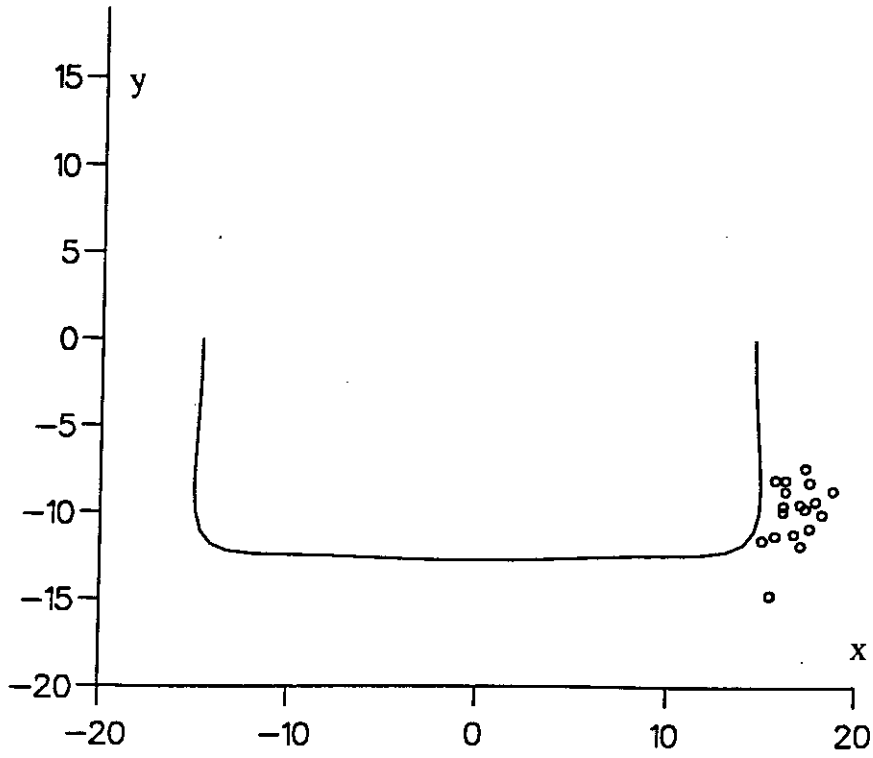

(c) Vortex Sheet at s=-0.16L

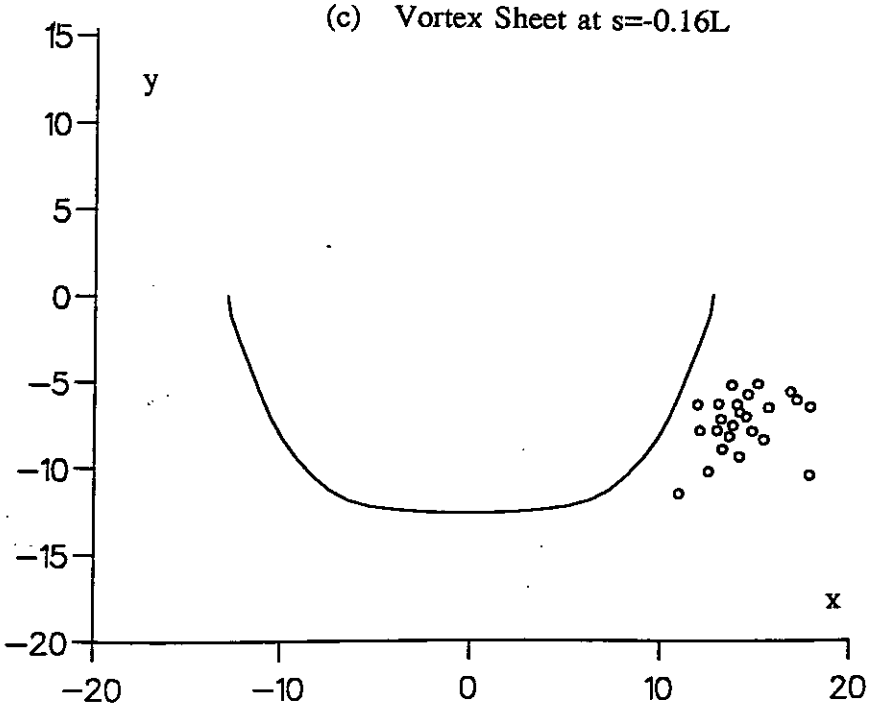

(d) Vortex Sheet at s=-0.40L

Fig.17 Vortex Sheets at Various Sections on The British Bombardier Hull (drift angle=4.0 degs.)

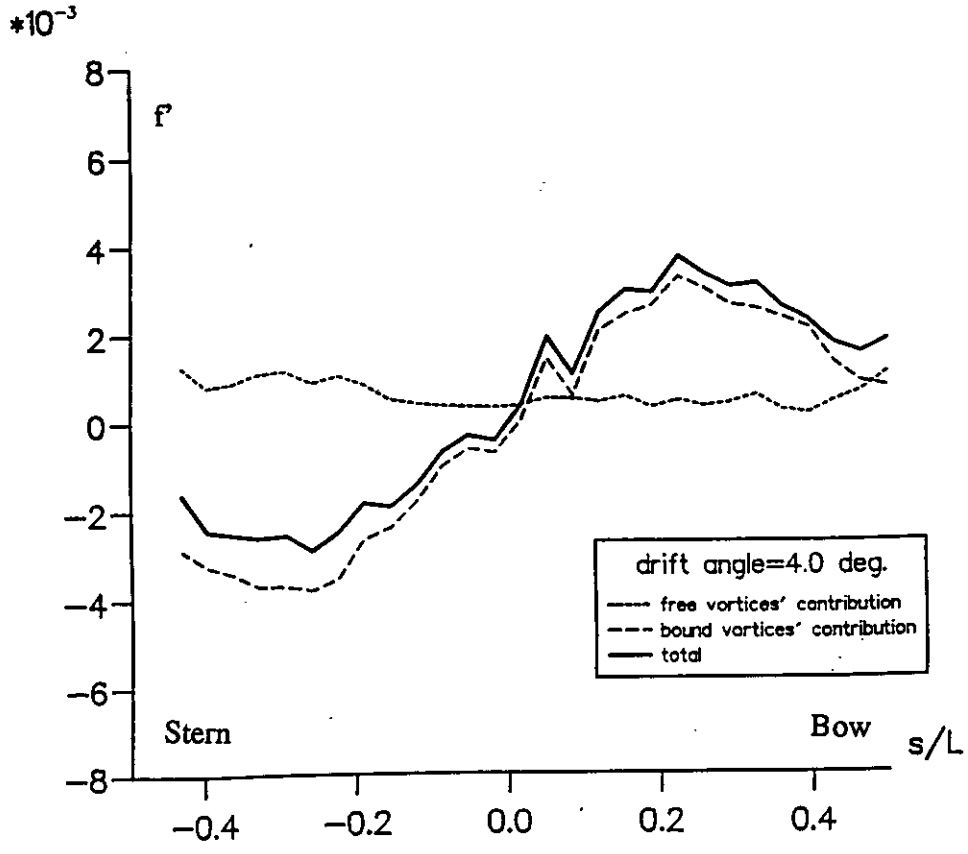

(a) Drift Angle=4.0 degs.

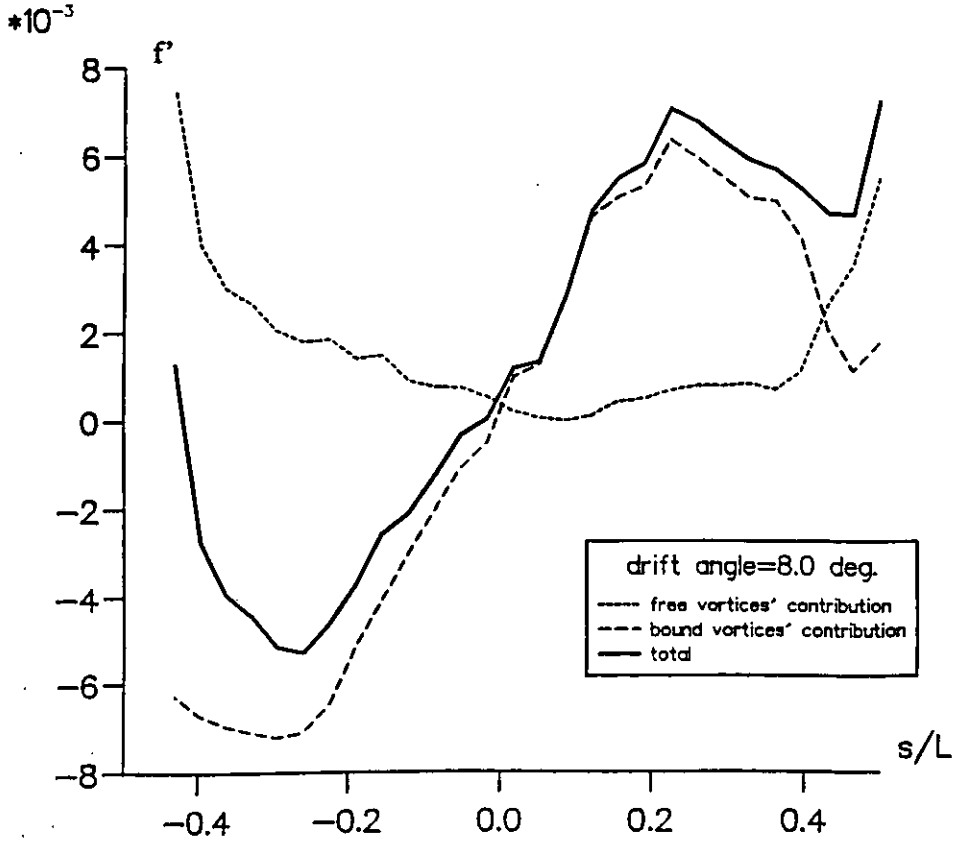

(b) Drift Angle=8.0 degs.

Fig.18 Calculated Side Force Distributions on The Mariner Hull

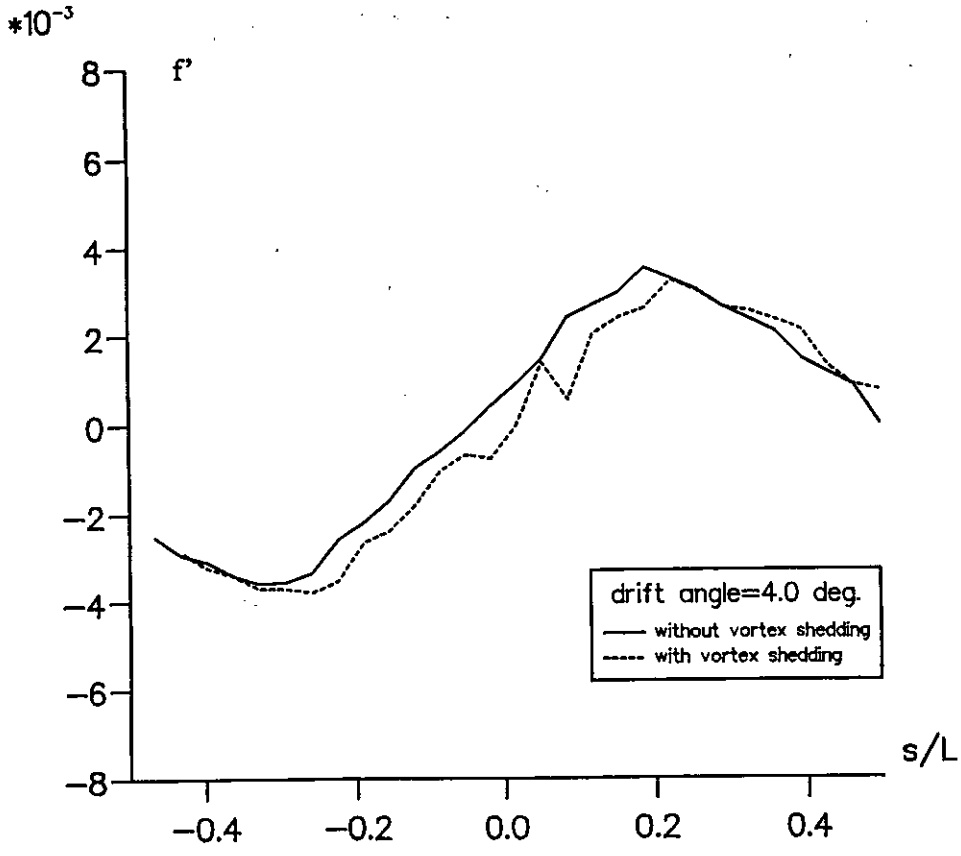

(a) Drift Angle=4.0 degs.

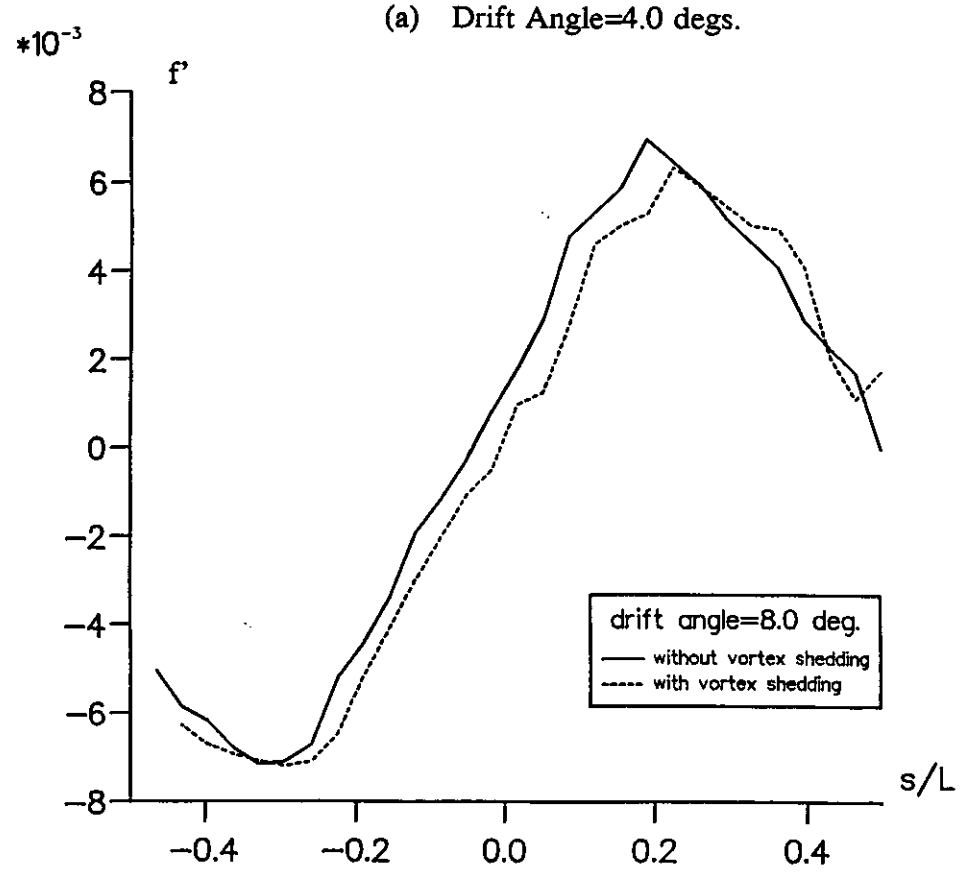

(b) Drift Angle=8.0 degs.

Fig.19 Effect of Free Vortices on Side Force Distributions Due to Bound Vortices

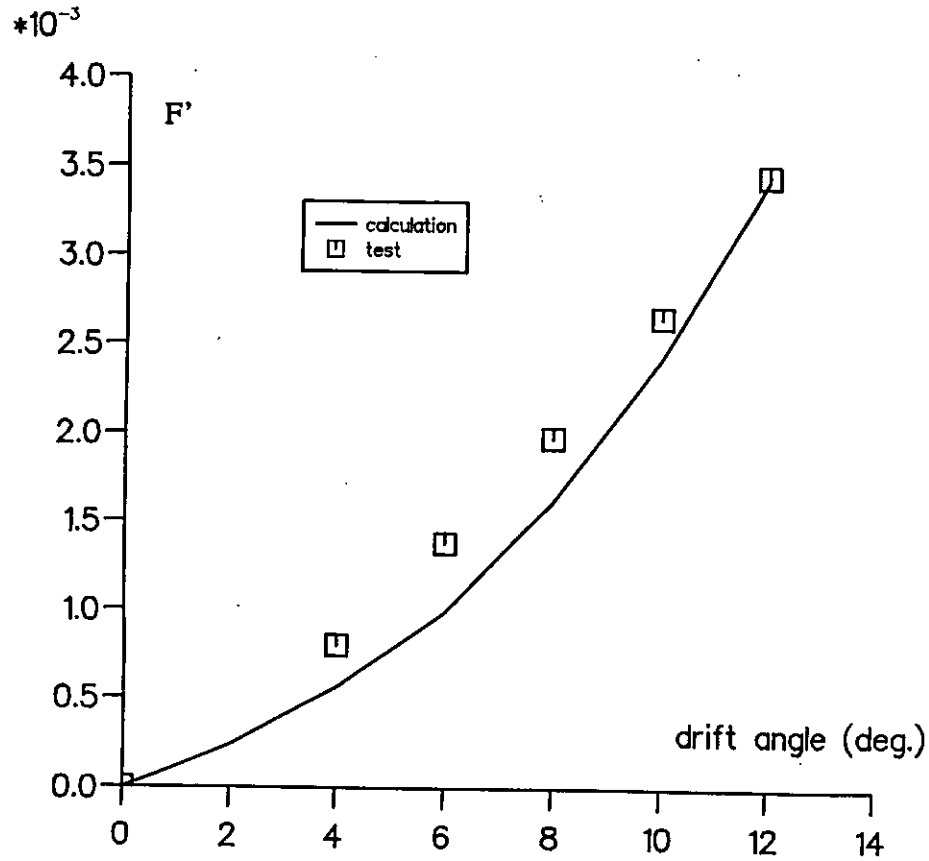

Fig.20 Comparison of Calculated Side Force with PMM Test for The Mariner Model (without using panel method in the calculation)

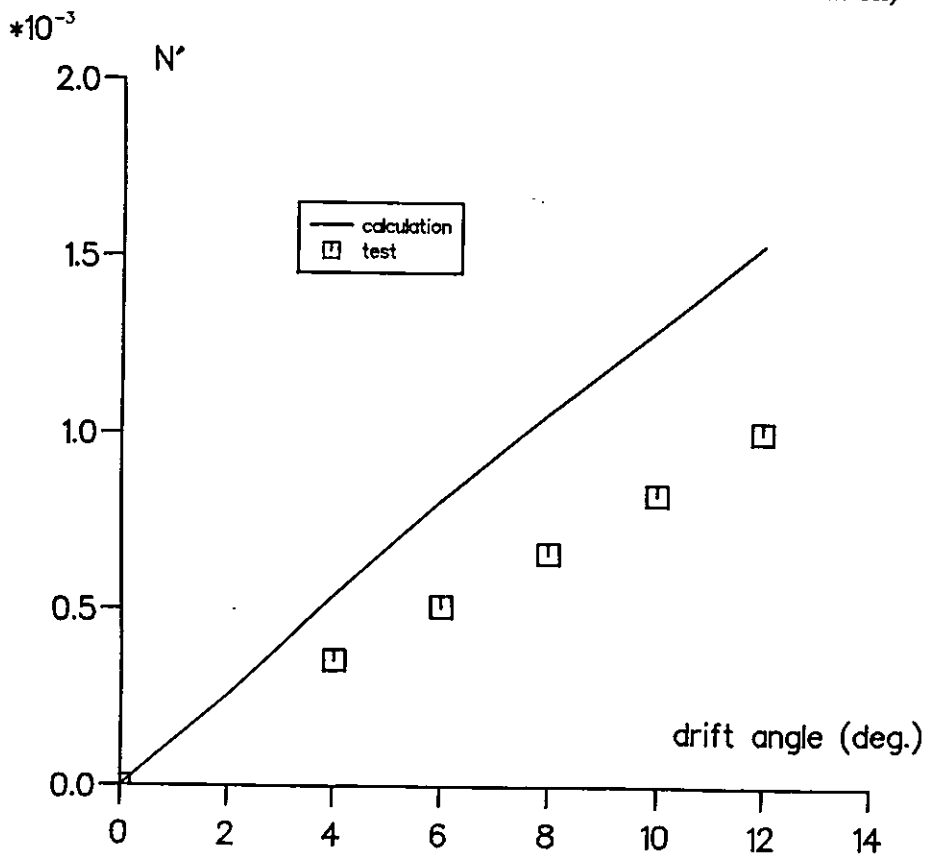

Fig.21 Comparison of Calculated Yaw Moment with PMM Test for The Mariner Model (without using panel method in the calculation)

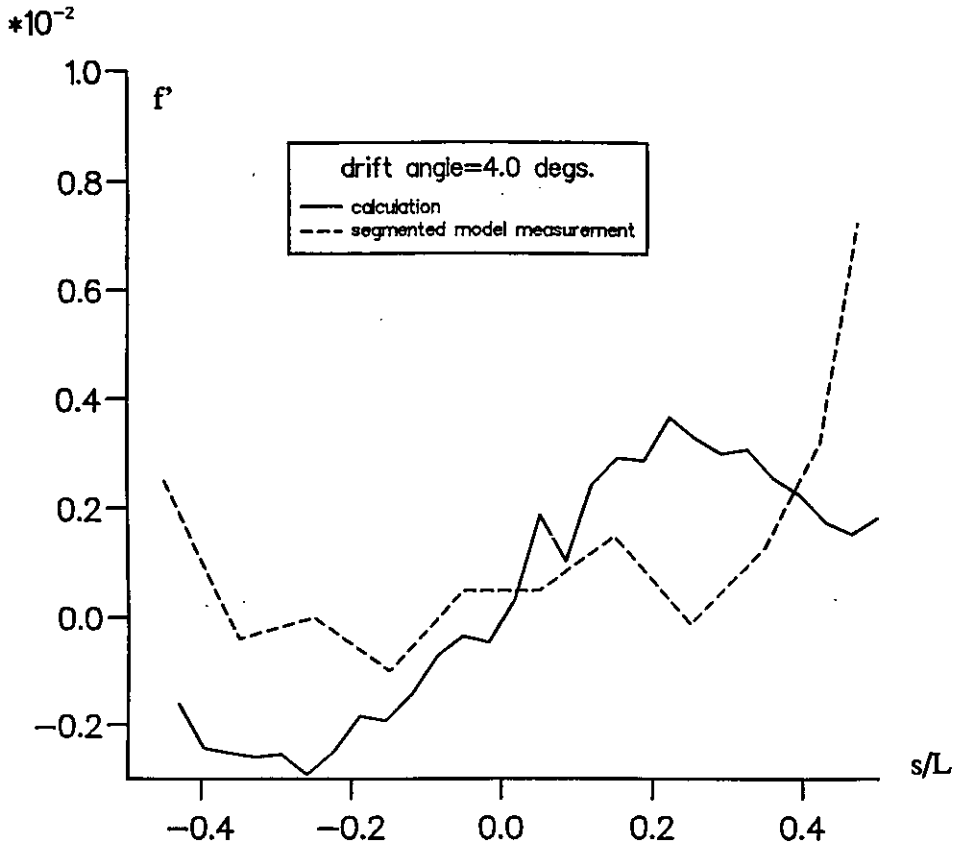

Fig.22 Comparison of Calculated Side Force Distribution with Segmented Model Test for The Mariner Model (without using panel method in the calculation)

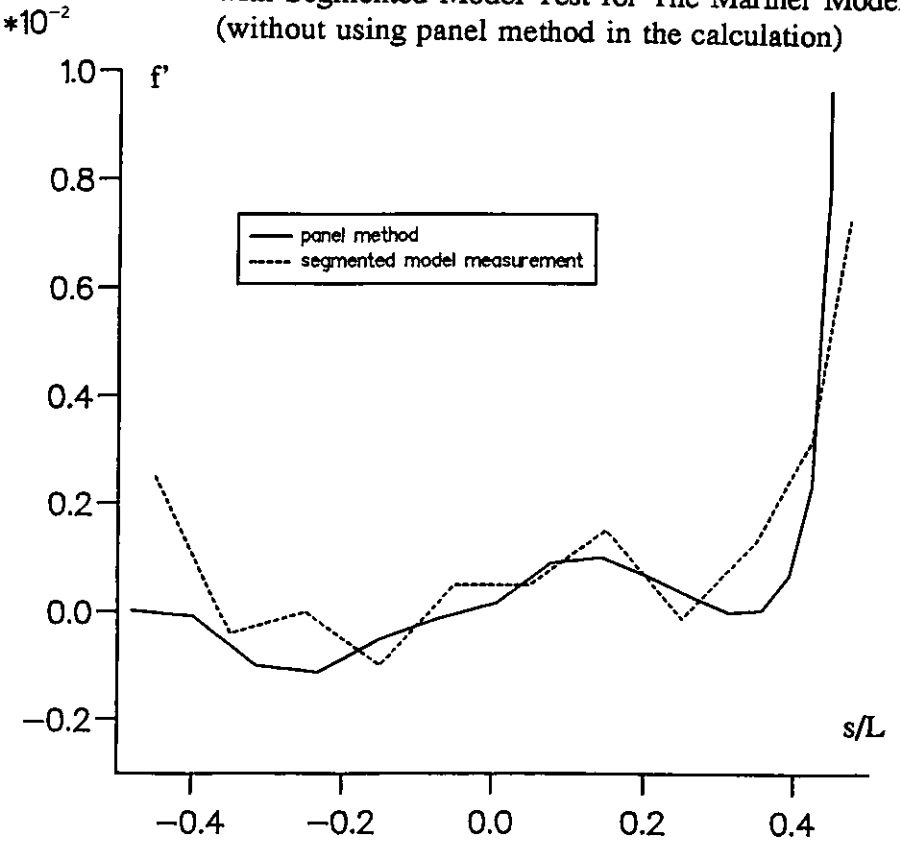

Fig.23 Comparison of The Calculation using Panel Method only with The Segmented Model Test for The Mariner Model (drift angle=4.0 degs.)

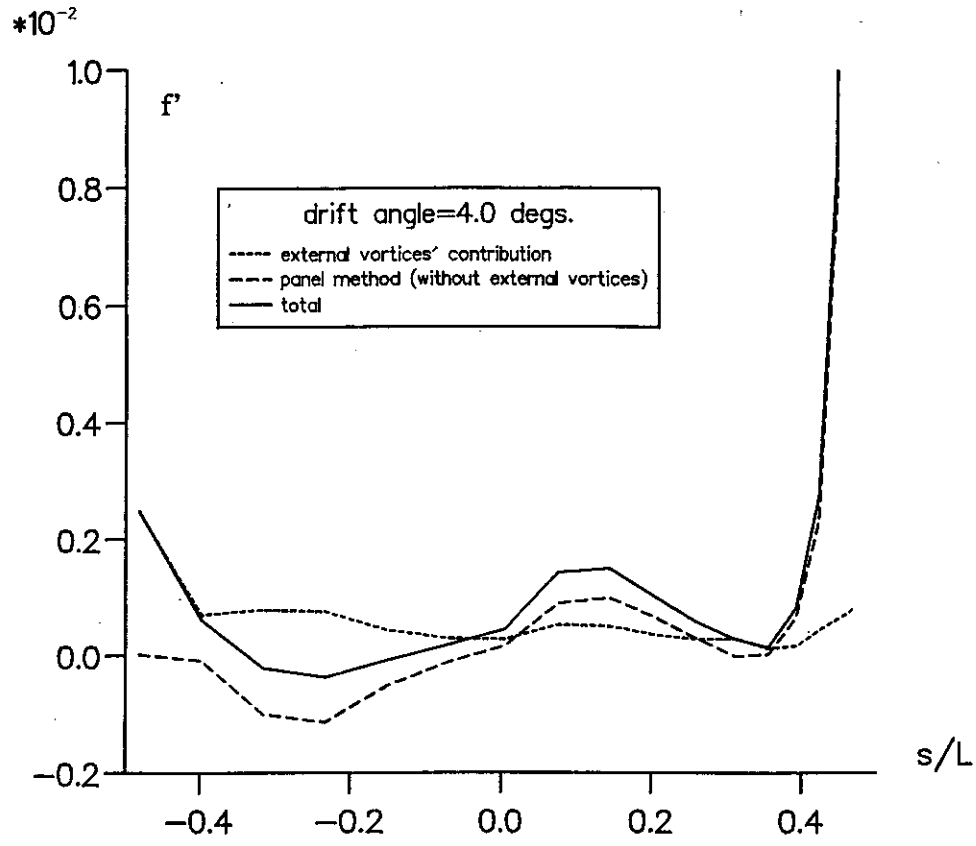

Fig.24 Comparison of Side Force Distributions on The Mariner Hull

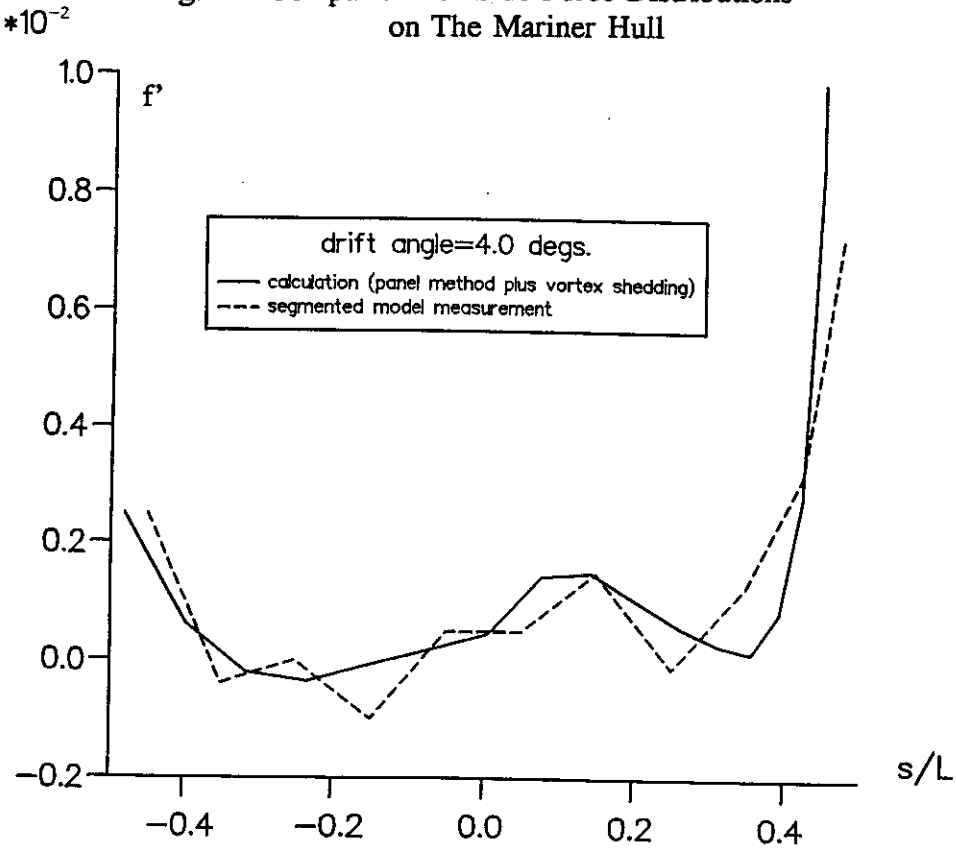

Fig.25 Comparison of Side Force Distributions on The Mariner Hull

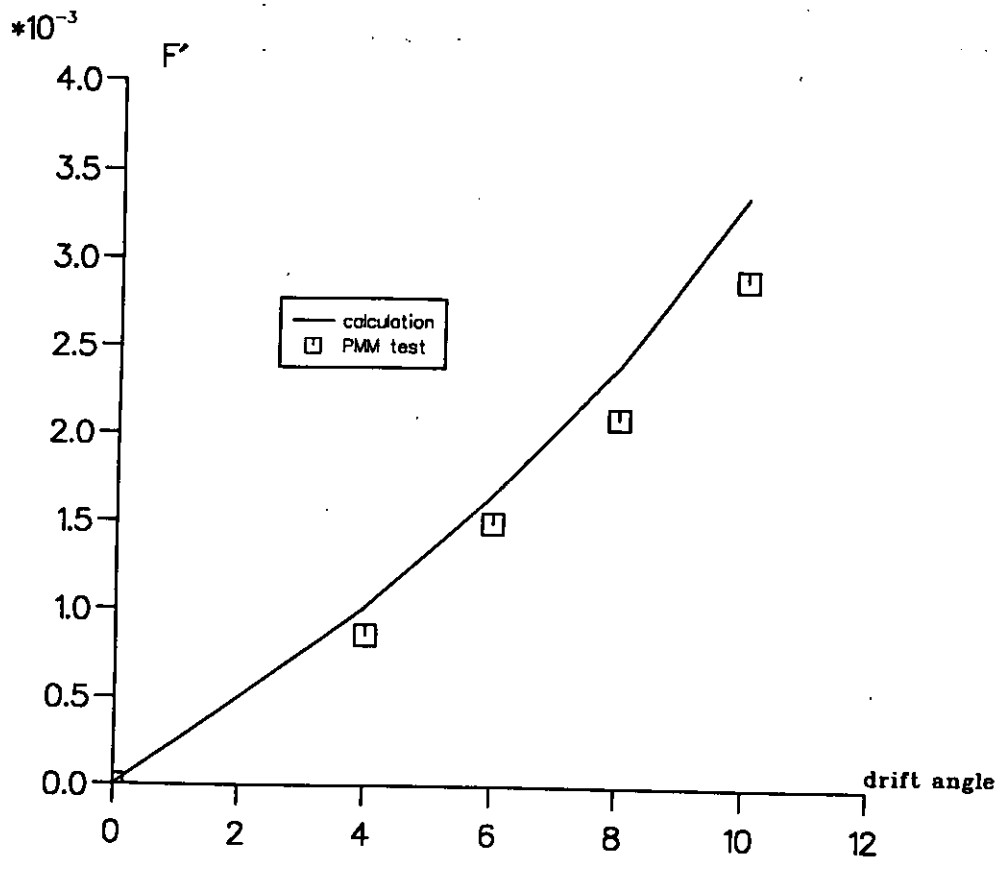

Fig.26 Comparison of Calculated Side Force with PMM Test for The Mariner Hull
(both vortex shedding and panel method were used in the calculation)

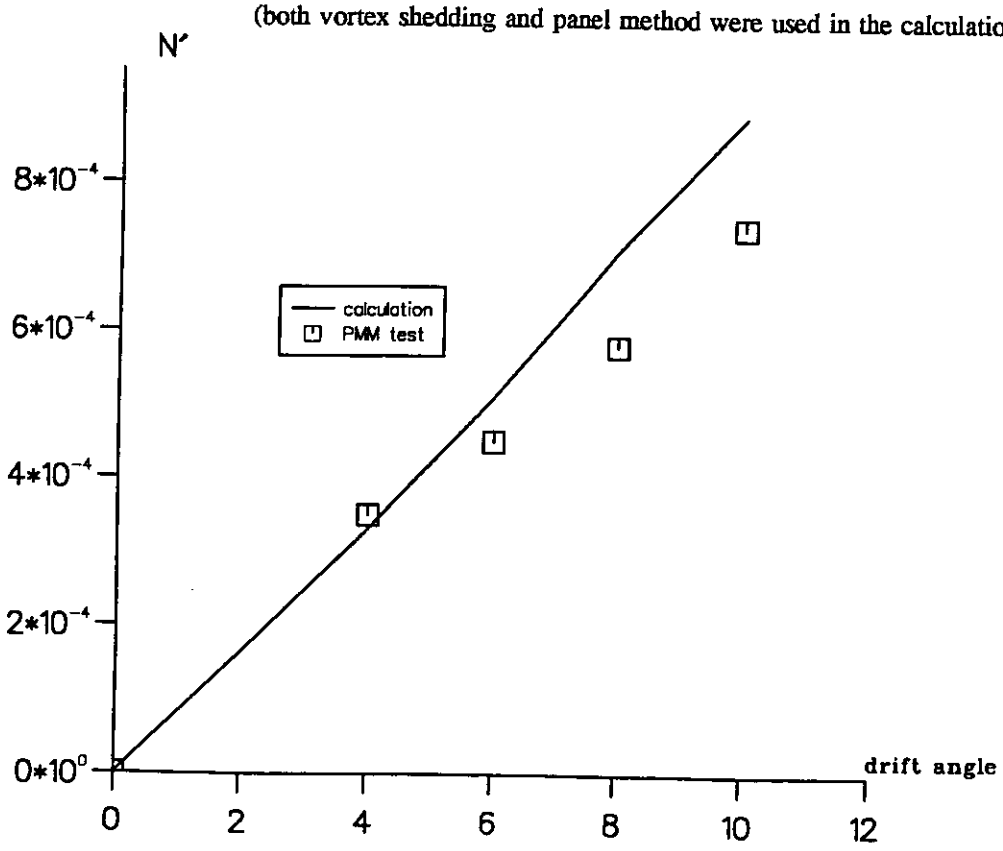

Fig.27 Comparison of Calculated Yaw Moment with PMM Test for The Mariner Hull
(both vortex shedding and panel method were used in the calculation)

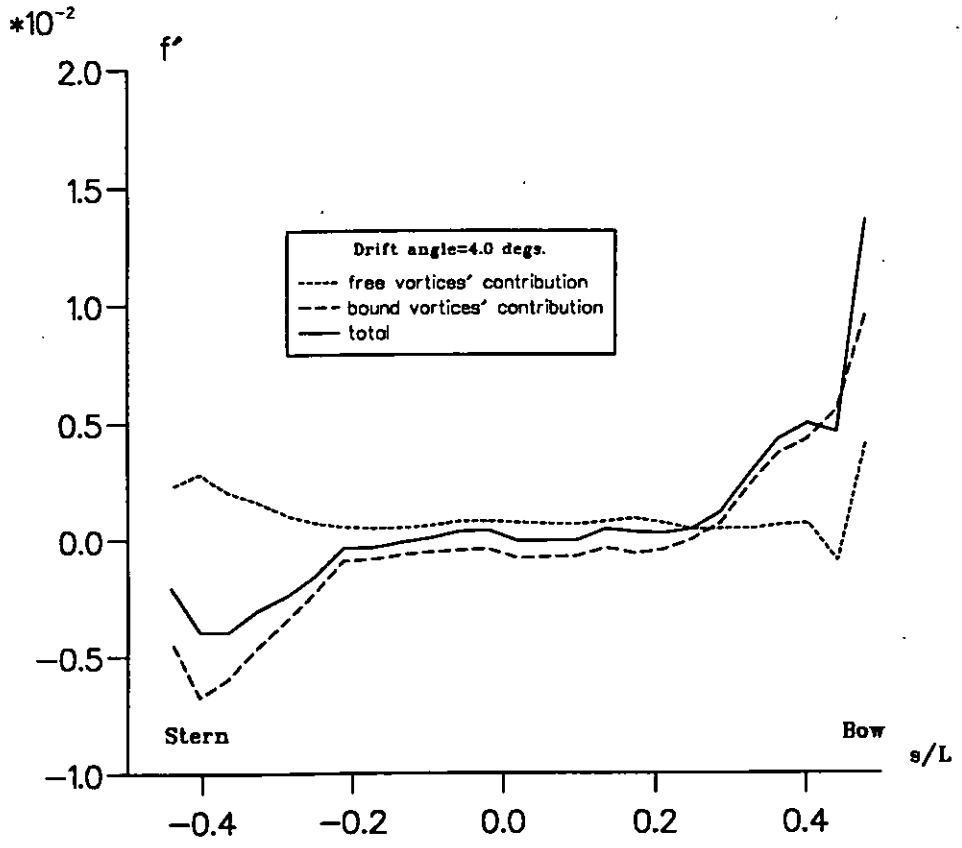

Fig.28 Calculated Side Force Distribution on The British Bombardier Hull

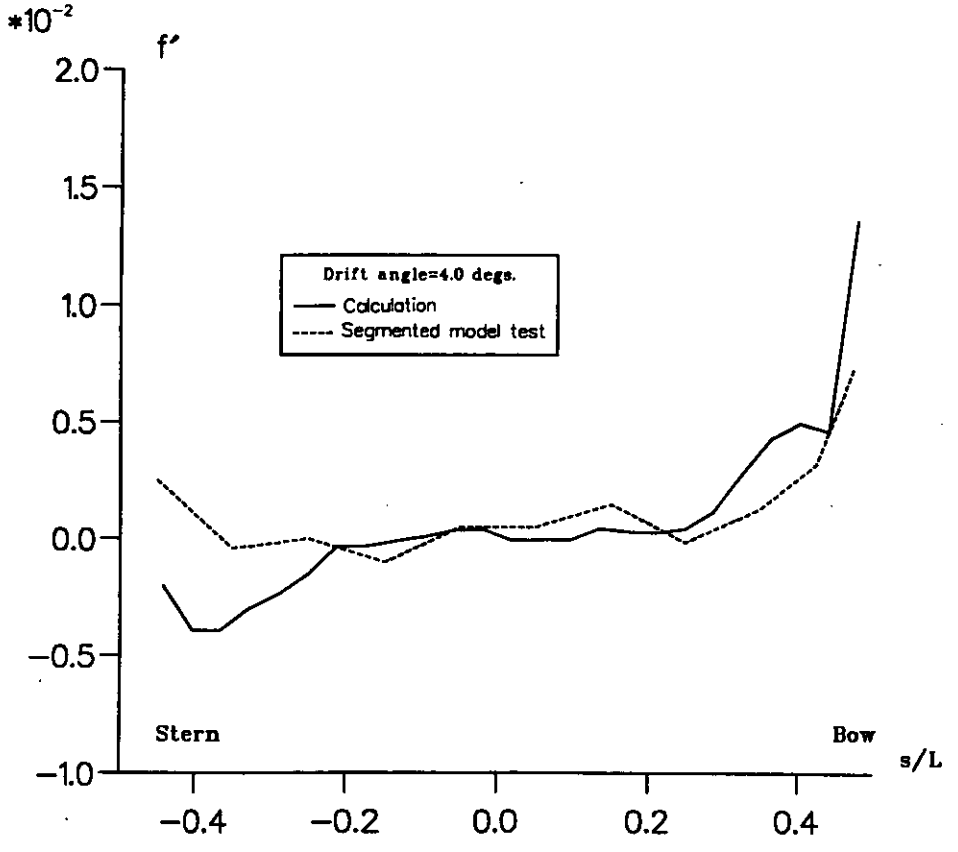

Fig.29 Comparison of Calculated Side Force Distribution with Segmented Model Test for The British Bombardier Hull

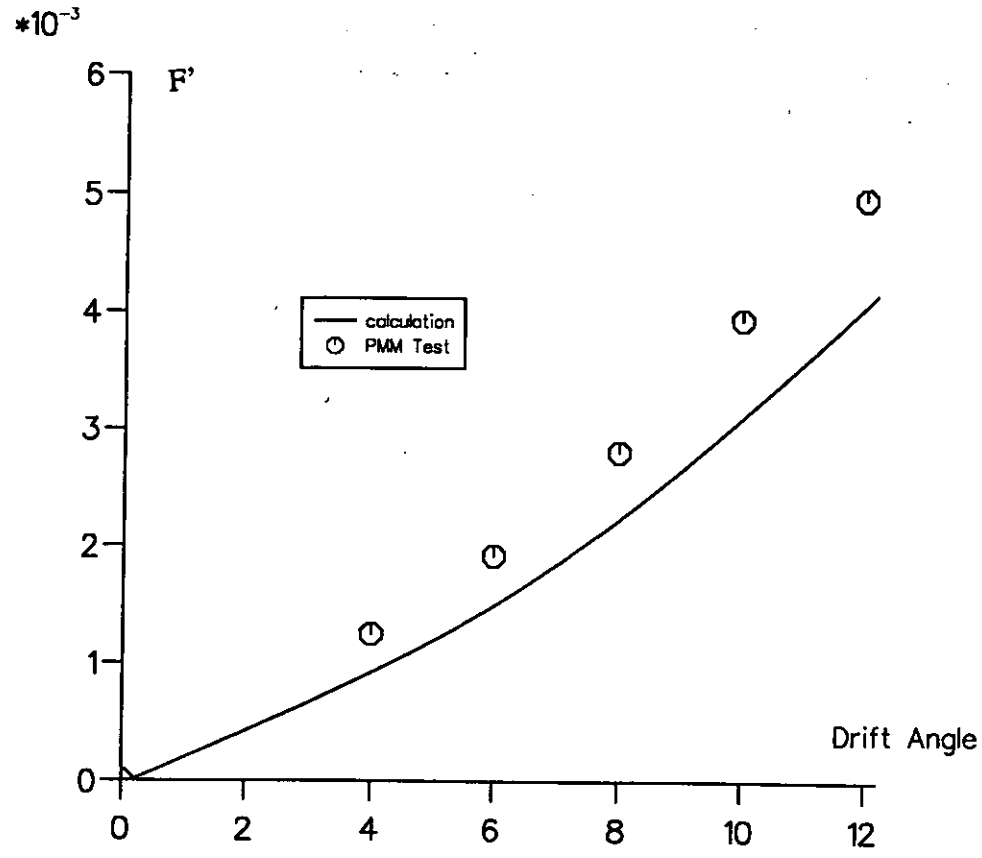

Fig.30 Comparison of Calculated Side Force with PMM Test for The British Bombardier Hull

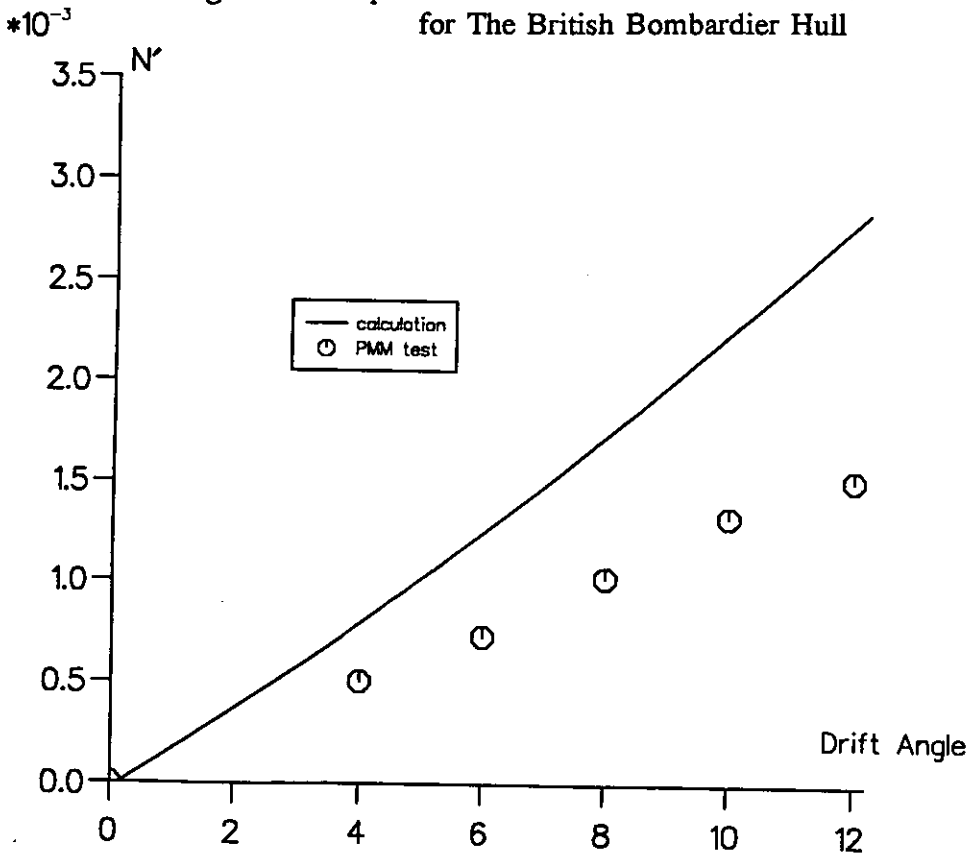

Fig.31 Comparison of Calculated Yaw Moment with PMM Test for The British Bombardier Hull